NAL TM-709T

ISSN 0452-2982
UDC 629.7.054
681.787.7

# 航空宇宙技術研究所資料

TECHNICAL MEMORANDUM OF NATIONAL AEROSPACE LABORATORY

TM-709T

# A New Configuration of Low-Cost Moderate Grade I-FOF Derived from JG-108FA

Sandra RAY・Masatoshi HARIGAE・Hirokimi SHINGU・Kazuhiro SAKUMA

1997年3月

航空宇宙技術研究所

NATIONAL AEROSPACE LABORATORY

# A New Configuration of Low-Cost Moderate Grade I-FOG Derived from JG-108FA

Sandra Ray*[1], Masatoshi Harigae*[2], Hirokimi Shingu*[2] and Kazuhiro Sakuma*[3]

## ABSTRACT

The aim of this research is to propose a new configuration of a low-cost moderate grade I-FOG for mass production. The theoretical part of this report mainly emphasizes the required reciprocity and the limitations of I-FOG. The experimental part describes the assembling and testing of four different gyro configurations derived from a moderate grade open-loop I-FOG produced by Japan Aviation Electronics Ltd., JG-108FA. Finally, by analyzing the tests data, we identify the different error sources generated in each case and establish a production cost-performance balance in order to apply a lower cost configuration for mass production.

This research was done by Ms Sandra Ray as her technical training under NAL in cooperation with Japan Aviation Electronics Industry, Ltd. from April 5 to August 23 in 1996.

**Keywords:** interferometric FOG, reciprocity, low cost, moderate grade

## 概　　要

本研究の目的は，低価格で大量生産が可能な民生用干渉型光ファイバージャイロの新しい構成法を提案することである。まず，光ファイバージャイロの原理を考察し，光の相対伝播特性（reciprocity）が大切であることと，ジャイロの性能を制限する種々の要因について述べる。つぎに，日本航空電子工業　製のJG-108FAをモデルベースに，4つのジャイロ構成法を提案し，それぞれ性能を実験的に評価する。その結果，価格と性能のバランスが取れた，大量生産可能な新しい光ファイバージャイロの構成法を提案することができた。

本研究は，サンドラ・レイが航技研における技術研修として行ったもので，日本航空電子工業　の協力を得て，1996年4月5日から8月23日までの期間にわたり実施した。

## Introduction

The measurement of rotation is of considerable interest in a number of areas. The popular rotation sensor over the past few decades has been the mechanical gyroscope which basically depends on the high angular momentum generated by a spinning wheel or a spinning ball. The advent of the laser in 1960 rekindled the interest in the use of the Sagnac effect for detecting the inertial rotation by purely optical means. Nowadays ring laser gyro technology has reached its full maturity and is used in many areas of inertial navigation. Twenty years ago, the development of low-loss optical fibers and solid state semi-conductor light sources and detectors opened up a very active and very promising area of research in fiber-optic rotation sensors also based on

＊　平成8年9月27日受付（received September 27. 1996）
＊1　制御部研修生，フランス国立航空宇宙高等大学校（Technical trainee, ENSAE in France）
＊2　制御部（Control Systems Division）
＊3　日本航空電子工業　（Japan Aviation Electronics Industry, Ltd.）

the Sagnac effect. The Interferometric Fiber-Optic Gyro (I-FOG) is now recognized as a crucial technology for many applications of inertial guidance and navigation. Its main advantages are : low-mass solid-state configuration, long lifetime, high reliability, high dynamic range, ability to withstand shocks and vibrations, large bandwidth, short warm up time and low power consumption.

From the physicist's point of view, the I-FOG brought many simple solutions to apparently complex problems, making high performance possible despite the various imperfections of the components. As a new technology, the I-FOG brings great expectations of very significant production cost reduction by using components that can be mass-produced.

Based on these two remarks, we shall first give a brief and simple derivation of the Sagnac effect in a vacuum and also in a medium, present the general configurations of I-FOG, discuss the necessity of reciprocity and polarization control together with their technical solutions. Other error sources will then be considered with emphasis on their technical solutions and their influence on the gyro performance. Once these theoretical basis are established, we shall present the results of our experimental research. We aimed at production of a low-cost moderate grade I-FOG, derived from JG-108 FA, using a new configuration technique. Therefore, the four different cases we chose to analyze will be compared in terms of performance, error sources and production cost so as to find the appropriate compromise for mass production.

## 1. PRINCIPLE OF THE INTERFEROMETRIC FIBER-OPTIC GYRO

### 1.1 Sagnac effect

Interferometric Fiber-Optic Gyro (I-FOG) measures input angular rate through the Sagnac effect. Detection of rotation with light was demonstrated by Sagnac in 1913. The Sagnac effect creates a differential phase shift between two beams of light counter-propagating in an optical fiber coil due to an input rotation rate. The Sagnac effect can easily be explained in the simple case of an ideal circular path (cf. Fig. 1).

Light entering the loop is divided into two counter-propagating waves that return in phase at point M after having traveled along the same path in opposite directions. In the case of rotation, during the transit time through the loop, the beam splitter has moved to M'. So, an observer, at rest in the inertial frame, sees that the co-rotating wave has had to propagate over a longer path than the counter-rotating one. The path length difference between the co-rotating wave and the counter-rotating one is given by :

$$\Delta L = c\Delta t \tag{1}$$

with

$$\Delta t = t_r - t_{cr} = 4\,\frac{\pi R^2 \Omega}{c^2} \tag{2}$$

where $t_r\,(= L/(c - R\Omega))$ and $t_{cr}\,(= L/(c + R\Omega))$ are the transit times of the co-rotating and counter-rotating waves, $c$ is the velocity of light in vacuum, $R$ is the radius of the circular path and $\Omega$ is the input rotation rate component parallel to the optical path input axis.

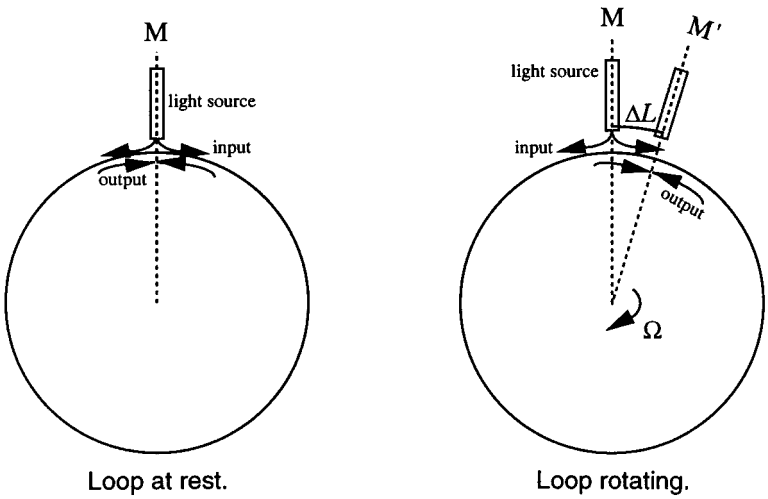


Fig. 1 Sagnac effect in the case of a circular path

Measured by interferometric means, this transit time difference yields the phase difference :

$$\Delta\phi = \frac{4\pi R^2\omega}{c^2}\,\Omega \tag{3}$$

where $\omega$ is the angular frequency of the wave.

This result is very general and can be extended to any axis of rotation and to any closed path, even if they are not contained in a plane, using a scalar product:

$$\Delta\phi = \frac{4\omega}{c^2}\,\mathbf{A}\cdot\Omega \tag{4}$$

where $\Omega$ is the rotation rate vector and **A** is the equivalent area vector of the closed path. The Sagnac effect appears as the flux of the rotation vector $\Omega$ through the enclosed area.

### 1.2 Sagnac effect in a medium

If light propagates in a medium, it can be demonstrated that the Sagnac induced phase shift remains unchanged (relativistic effect).

In the case of light propagation in a medium of index n, the velocity of propagation must take into consideration the relativistic addition of the velocity of light in the medium, i.e., $c/n$ and the tangential velocity of the medium, i.e., $R\Omega$ so that the velocity of the co-rotating wave, $c_r$ becomes :

$$\begin{aligned} c_r &= \frac{\frac{c}{n}+R\Omega}{1+\frac{R\Omega}{nc}} \\ &\cong \frac{c}{n}+R\Omega\left(1-\frac{1}{n^2}\right) \end{aligned} \tag{5}$$

to the first order in $\frac{R\Omega}{c}$. Similarly, the velocity of the counter-rotating wave, $c_{cr}$, is given by:

$$\begin{aligned} c_{cr} &= \frac{\frac{c}{n}-R\Omega}{1-\frac{R\Omega}{nc}} \\ &\cong \frac{c}{n}-R\Omega\left(1-\frac{1}{n^2}\right)\cdot \end{aligned} \tag{6}$$

Therefore, $\Delta t$ in the medium becomes :

$$\begin{aligned} \Delta t &= t_r - t_{cr} \\ &= 2\pi R\,\frac{2R\Omega-(c_r-c_{cr})}{c_r c_{cr}}\cdot \end{aligned} \tag{7}$$

Upon substitution for $c_r$ and $c_{cr}$ from above, we get :

$$\begin{aligned} \Delta t &= 2\pi R\,\frac{2R\Omega-2R\Omega\left(1-\frac{1}{n^2}\right)}{\frac{c^2}{n^2}} \\ &= 4\pi R^2\,\frac{\Omega}{c^2} \\ &= \frac{4}{c^2}\mathbf{A}\cdot\Omega \end{aligned} \tag{8}$$

which is identical to that in a vacuum.

The transit time difference does not depend on the index n. As a consequence, the phase shift is also independent from n.

### 1.3 Interferometric Fiber-Optic Gyro

(1) Principle

The basic configuration of an I-FOG includes a light source, a optical fiber coil and a detector as shown in Fig. 2. The light source is coupled into the input of a coupler. The outputs of the coupler are fed into the two ends of the fiber coil and circulate in opposite directions. After the light waves pass through the fiber coil, they are coupled back through the coupler. The light is then directed onto the detector and is used to extract phase information proportional to input rotation rate. In the case of input rotation rate, a differential phase shift is created between the two beams of light counter-propagating in the optical fiber.

The differential phase shift $\Delta\phi$ corresponds to a shift of interference fringes from their initial position given by :

$$\Delta z = \frac{\Delta\phi}{2\pi} = \frac{\Delta L}{\lambda}\cdot \tag{9}$$

That is to say :

$$\Delta z = 4\,\frac{\mathbf{A}\cdot\Omega}{c\lambda}\cdot \tag{10}$$

Intensity of the light in the observation point is a function of the rotation rate.

$$I = I_0(1+\cos\Delta\phi)$$

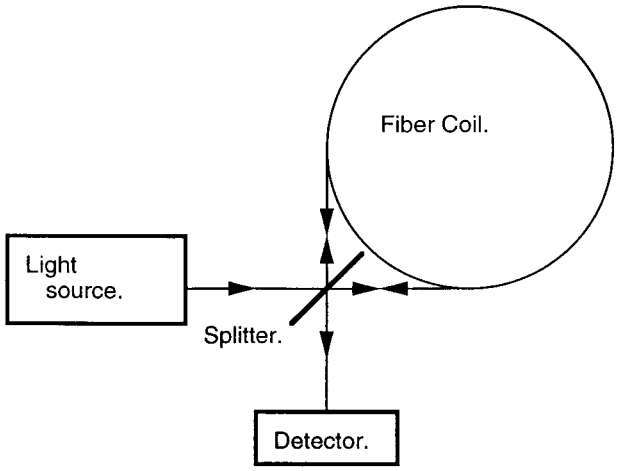


Fig. 2 Basic configuration of I-FOG

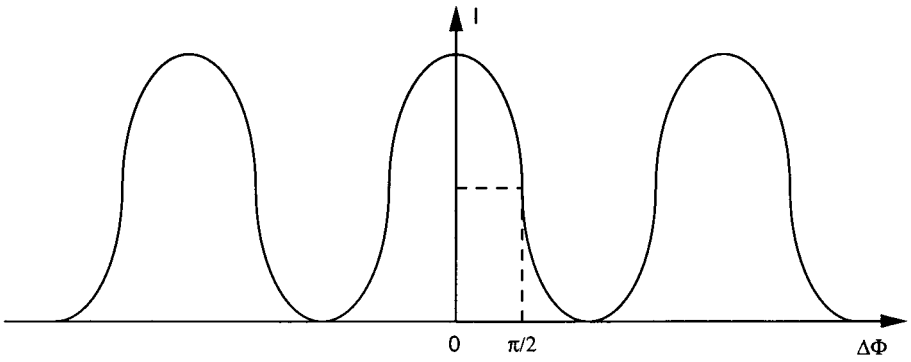


Fig. 3 Natural response of I-FOG

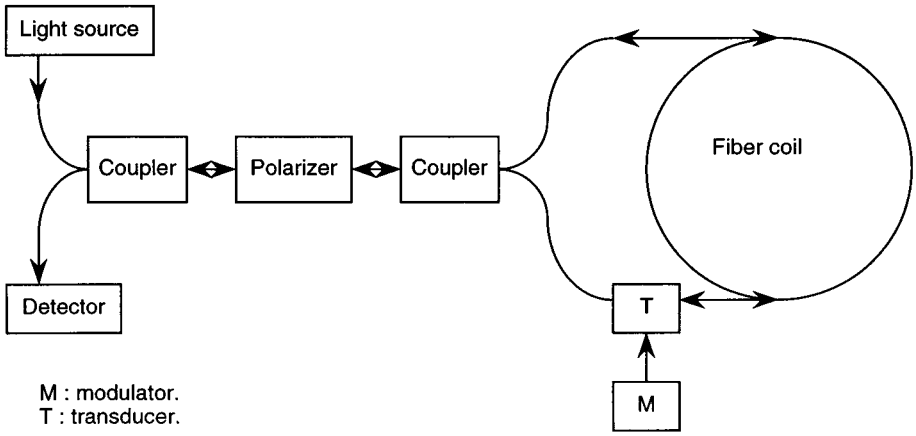


Fig. 4 Open-loop configuration

$$= I_0\left(1 + cos\left(\frac{8\pi}{c\lambda}\mathbf{A}\cdot\Omega\right)\right) \tag{11}$$

The Sagnac induced phase shift is enhanced by using a multiturn optical fiber coil. The influence of the number of turns $N$ in the coil is given by:

$$\Delta\phi_N = N\frac{8\pi}{c\lambda}\mathbf{A}\cdot\Omega. \tag{12}$$

Sensitivity appears as proportional to $N$. Nevertheless, fiber length is limited by attenuation. I-FOG uses, as waveguide, a coil of optical fiber of several hundreds meters length. It can achieve good performance rate sensing in small package volume.

As in any passive optical system, the theoretical sensitivity of I-FOG is limited by the photon shot noise. Sensitivity is maximized by operating with a phase bias of $\pi/2$ (cf. Fig. 3) and then the photon shot noise limitation is significantly reduced. The minimum response time of I-FOG is the transit time through the fiber coil. This yields a very high theoretical bandwidth (several hundreds of kilohertz). Even if the signal processing techniques reduce this bandwidth, frequency ranges of several kilohertz are reached, which is a very significant improvement over previous technologies.

(2) Open-loop configuration

The natural response of the gyro is non-linear and with a poor sensitivity. Indeed, the natural gyro is operated with a nominal zero path difference and, as shown in Fig. 3, for small variations in relative phase, there is negligible variation in the intensity output. Open-loop configuration (cf. Fig. 4) achieves better linearity and higher sensitivity using bias modulation with a phase bias of $\pi/2$.

Suppose modulation voltage is given by Fig. 5 and consider the beams of light entering the coil at t-$\tau$, where $\tau$ is the transit time through the coil.

- The counterclockwise wave immediately goes through T. So, its phase bias shift is given by kV(t-$\tau$) with k constant.
- The clockwise wave passes through the coil before going through T at t. So, its bias phase shift is given by kV(t).
- Finally, when the two beams of light recombine, the cumulated bias phase shift is k(V(t)-V(t-$\tau$))=2kV(t).

The interferometric signal is modulated. Fig. 6 describes how this modulation puts the operating points on a relatively linear part of the interferometer characteristic $I(\Delta\phi)$. In the case of

no rotation, the bias phase shift $\pm$ kV(t) places the operating points in $M+$ and $M-$ and then results in a constant intensity of the output signal. In the case of rotation, the operating points move to opposite sides of $M+$ and $M-$. It results in a modulation of the interferometer output signal $s(t)$. If rotation rate $\Omega$ is not too high, nearly linear part of the interferometer characteristic is used and intensity tends to be proportional to rotation rate $\Omega$.

A phase modulator can be realized, for example, by using the elasto-optic effect. The fiber is wrapped around a cylinder of piezoelectric material in several turns. If an alternating voltage is applied to the piezoelectric cylinder, mechanical vibrations are generated. The phase of the light wave passing through the fiber is then modulated via the elasto-optic effect. This arrangement is the preferred solution for all-fiber gyroscopes. If Integrated-Optic Components are used, it is advantageous to use an electro-optic substrate, e.g., $LiNbO_3$. With two electrodes adjacent to the waveguide, an electrical field is induced inside the waveguide and the phase of the light is modulated.

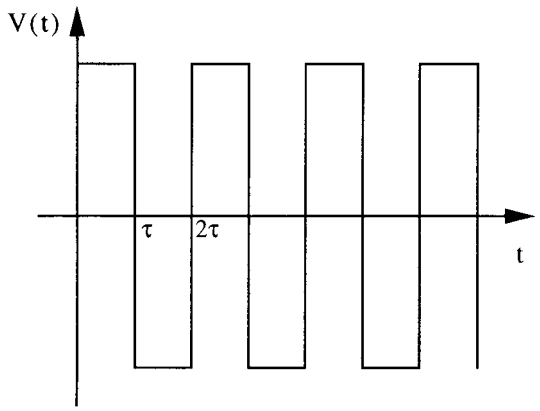


Fig. 5 Modulation voltage

(3) Closed-loop configuration

Open-loop configuration is criticized for its intrinsic sinusoidal output function with rate and for its low dynamic range. This technology is also sensitive to changes in optical power, modulation depth, changes in overall optical path loss and electronic drifts. As a result, most I-FOG developments have opted for a closed-loop signal processing approach based on the superior scale factor stability and linearity associated with operating the Sagnac interferometer at a null.

In the closed-loop configuration (cf. Fig. 7), the output of the demodulator is passed through a servo amplifier which then drives a non-reciprocal phase transducer (NRPT) placed within the fiber coil. In this way, the interferometer is always operated at null, i.e., at $\Phi_{s-c} = 0$ by generating a suitable non-reciprocal phase shift in the NRPT that is equal in magnitude to but opposite

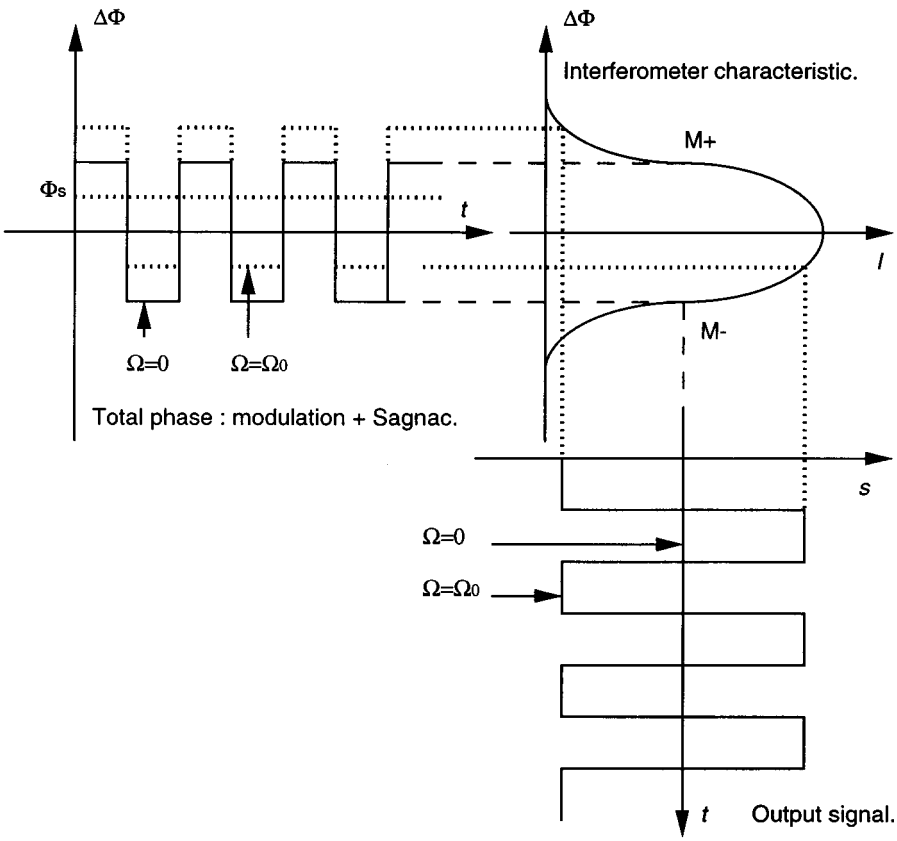


Fig. 6 Modulation fo the interferometric signal

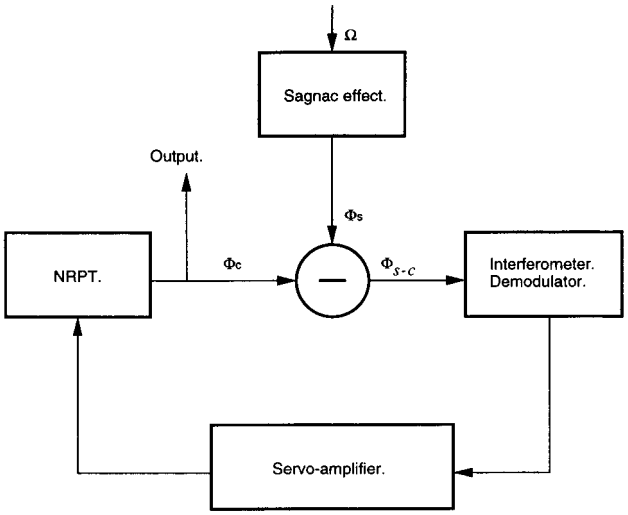


Fig. 7 Closed-loop principle

in sign to the Sagnac induced phase shift. The output of the system is then the output of the NRPT.

## 2. RECIPROCITY OF AN I-FOG

Theoretical analyses of I-FOG led to the conclusion that this sensor could measure rotation rates of less than 0.01°/h. These analyses assumed that the limiting noise is shot noise at the photodetector. This sensitivity range would permit I-FOG to be used as a navigation grade gyro in competition with laser gyros and conventional spinning-mass gyros. The experimental results demonstrated sensitivities much worse than those predicted by the theoretical analyses. It appeared that experimental sensitivities were not limited by shot noise but rather by reciprocal noise in the fiber coil and other parts of the optical path. This reciprocal noise can be greatly reduced by ensuring that the interferometer uses only a single polarization state in a single-mode birefringent fiber.

### 2.1 Principle of reciprocity

In a linear medium, the propagation equation of the wave amplitude A is :

$$\nabla^2 A - \frac{n^2}{c^2}\frac{\partial^2 A}{\partial t^2} = 0. \qquad (13)$$

Looking for harmonic solutions, $A(x,y,z,t) = A_s(x,y,z)e^{i\omega t}$, where depends only on the spatial coordinates and is the angular frequency, the propagation equation is reduced to:

$$\nabla^2 A_s + \frac{n^2\omega^2}{c} A_s = 0. \qquad (14)$$

Therefore, any solution $A(x,y,z,t) = A_s(x,y,z)e^{i\omega t}$, has a perfectly reciprocal solution $A'(x,y,z,t) = A_s(x,y,z)e^{-i\omega t}$ since the reduced propagation equation depends on the square $\omega^2 = (-\omega)^2$. Physically, this mathematical change of sign corresponds to a propagation in the opposite direction with exactly the same propagation delay and the same attenuation of the phase front. In free space, difficult alignments are required to excite both reciprocal opposite solutions and it is never perfect. However, if the system is single-mode, alignments are only needed to optimize the whole power. Once it is coupled, both opposite waves are automatically reciprocal.

### 2.2 Reciprocal configuration

A simple fiber ring interferometer is not intrinsically reciprocal. Complementary interference fringes are observed at both ports of the interferometer, depending on the alignments of the fiber ends (cf. Fig. 8). At the input, the beam is split and focused on both fiber ends that filter the unique propagation mode and, at the output, the beams are recombined to interfere. A small change in the alignments has a significant effect on the matching of both output phase fronts, modifying the fringe pattern and, consequently, producing a variation proper to the measured phase difference. The Sagnac effect is a very small first-order effect in $R\Omega/c$ which is buried in the change of the zero-order, the absolute phase cumulated in the propagation. Fortunately, single-mode reciprocity provides perfect common-mode rejection and will permit the nulling out of this zero-order and its variations almost perfectly. So, to avoid this severe limitation and to get high performance, a so-called reciprocal configuration is used (cf. Fig. 9).

Light is fed into the interferometer through a truly single-mode waveguide and the returning interference waves are filtered through the same waveguide in the opposite direction. This simple modification has made both opposite paths identical, zero rotation giving zero phase difference. In this case, alignments are needed solely to optimize the whole power which requires difficult but reasonable mechanical tolerances. Spatially, a short length (about 1m) of single-mode fiber can be considered as a perfect filter. Nevertheless, there is also a need for polarization filtering, since a single-spatial-mode fiber is actually a dual-polarization-mode fiber and the fiber birefringence may yield a spurious phase difference.

In addition to the coil splitter, the complete reciprocal configuration needs a second splitter to tap off a part of the interference wave returning through the filtered input-output port of the ring interferometer. The power loss generated by this second splitter is the price paid to insure reciprocity in the optical system.

The use of a truly single-mode filter at the common input-output port of the interferometer renders the fiber ring interferometer sensitive only to non-reciprocal effects as the Sagnac

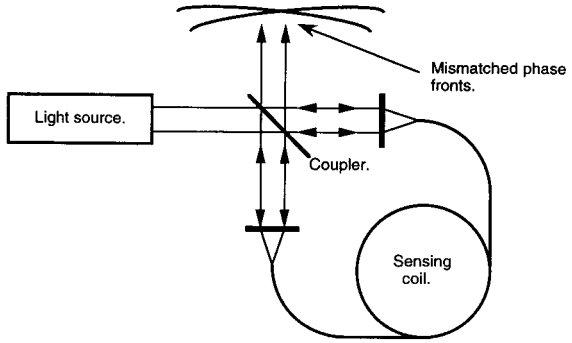


Fig. 8 Fiber ring interferometer

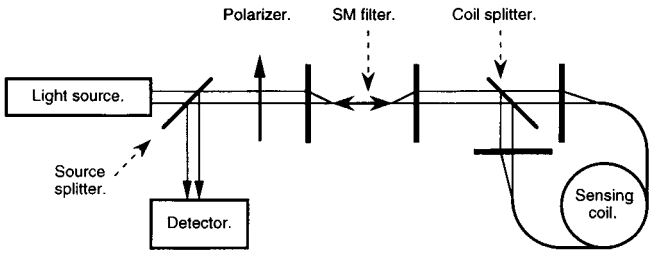


Fig. 9 Reciprocal configuration

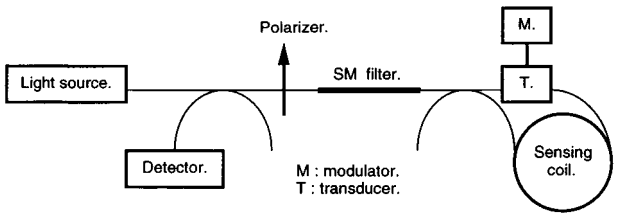


Fig. 10 Minimum reciprocal configuration

effect. Furthermore, a modulation-demodulation at the proper or eigenfrequency of the coil provides a biased signal that does not degrade the original perfection of the system. These two simple conditions, combined in a so-called minimum reciprocal configuration, make high performance possible despite the various defects of the components (cf. Fig. 10).

### 2.3 Polarization reciprocity

(1) Polarization errors

A Single-Mode (SM) fiber has actually two polarization-modes. The residual birefringence of a SM fiber modifies the polarization state as the light propagates. In the fiber coil, at a given position, both counter-propagating waves have different polarization states and therefore, because of birefringence, do not see exactly the same index of refraction. This yields a spurious phase difference at the output. It is possible to show that, theoretically, if a polarizer is placed at the common input-output of the fiber, the phases of the waves transmitted in opposite directions are then perfectly equalized. However, the rejection of a practical polarizer is not infinite and there remains a residual phase difference between both counter-propagating waves.

The first I-FOG were constructed using SM fiber. At that time, it became obvious that uncontrollable and environmentally dependent polarization evolution occurring in the SM fiber is manifested as bias drift and signal fading. Complete signal fading happens when the coil imparts a rotation of the polarization vector that places it in alignment with the extinction axis of the polarizer. It is then rejected by the polarizer and no light reaches the detector. To avoid the signal fading problem, the use of a depolarizer in the gyro loop was proposed and demonstrated.

Polarization Maintaining (PM) fiber, which appeared on the market in the early 80's, provided a simple mean of polarization control, preserving the simplicity of the gyro architecture. The use of PM fiber resulted in significant advances allowing today's I-FOG technology to offer navigation grade performance. Nevertheless, it complicated the cost problem. The early hopes that PM fiber, which is the highest cost item in the navigation grade gyro, would become inexpensive with time still remain unfulfilled. Due to the large volumes produced for use in optical communications and its simpler design, SM fiber is one to two orders of magnitude lower in cost than PM fiber. Nevertheless, SM fiber gyroscopes continue to be considered by most I-FOG developers as a technology only suitable for less demanding applications.

Polarization errors depend on the quality of the polarizer, on the amount of the polarization cross-coupling and the coherence between the interfering waves. The biggest step in overcoming problems with polarization errors was the introduction of the broad-band light source which provides substantial decorrelation for light waves taking paths different from the primary waves. Nevertheless, many of these sources have quite complex coherence functions and decorrelation of the cross-coupled waves is not always a straightforward task. The introduction of PM fiber greatly simplified polarization management as the same polarization state can be maintained throughout the gyro. Suppression of polarization errors in the depolarized gyro still remains challenging.

(2) PM gyroscopes

Two groups of polarization errors are identified: amplitude-type errors and intensity-type errors.

Intensity-type polarization errors mainly result from interference of two waves which cross-couple at the points $K_2$ and $K_3$ (cf. Fig. 11) and both propagate through the reject axis of the polarizer. Because of excellent polarizers that are available nowadays, intensity-type polarization errors are of little concern. Of primary concern are the amplitude-type polarization errors.

These errors result from the interference of a primary wave and a cross-coupled wave. The cross-coupled wave couples to the

"wrong" polarization in front of the polarizer at the point $\kappa_1$, propagates through the reject axis of the polarizer and cross-couples back to the "right" polarization within the sensing coil at the point $K_2$ or $K_3$. The primary wave then serves as a local oscillator for the coherent detection of this cross-coupled wave; that is why the amplitude type polarization errors yield a significant spurious signal compared to the intensity type errors. Therefore, minimization of the cross-coupling and use of a polarizer with high extinction ratio lead to the reduction of these errors.

The typical PM gyro with an IOC is constructed to guide linearly polarized light in the fast axis. So, the cross-coupled wave spends some time propagating in the slow axis and encounters a birefringence induced delay with respect to the primary wave. The adjustment of this delay and the use of a broad-band light source are additional very powerful techniques of polarization errors suppression. Indeed, the amplitude-type polarization errors $\phi_A$ are proportional to the degree of partial coherence $\gamma(\tau)$ of the light source and this discussion can be summarized in a very simple equation :

$$\phi_A \propto \kappa_1 \kappa_2 \varepsilon \gamma(\tau) \tag{15}$$

where, $\kappa_1$ $\kappa_2$ are the amplitude cross-couplings at the points $K_1$, $K_2$. $\varepsilon$ is the amplitude extinction ratio of the polarizer.

Nevertheless, many light sources have quite complex coherence functions. An example of a SLD's coherence function is shown in Fig. 12. A good gyro design should take into account all the cross-coupled delayed waves that interfere with the primary wave and lead to the polarization errors. The delays of the cross-coupled waves have to be adjusted so that their location on the coherence function provides sufficient decorrelation, i.e., delays have to be placed away from the coherence peaks, in the regions of low coherence.

The optimal operating conditions for polarization errors control can be summarized as follow:

- Use of the same optical axis throughout the gyro. The cumulated birefringence induced delays then move away from the coherence peaks.
- Use of an optical circuit and a sensing coil with high birefringence. Large delays are induced in this way and can eliminate many polarization errors.
- Use of a light source with a coherence function composed of few recorrelation peaks.

(3) Depolarized gyroscopes

The coil of the depolarized gyro can be made out of SM fiber. The polarization of the light in the SM coil undergoes evolution that depends on the environment, i.e., temperature, mechanical stresses, magnetic field, etc.

In order to avoid signal fading, the light must be depolarized within the gyro loop. This is accomplished by using single or dual depolarizers as shown in Fig. 13. Depolarizers are made out of PM fiber which is attached to the IOC or its leads at 45°. They have to be long enough to decorralate the light waves propagating in their slow and fast axis. Then, regardless of the polarization evolution within the coil, half the light always returns aligned with the pass axis of the polarizer and reaches the detector.

A quick inspection of the depolarized gyro architecture reveals many problems with polarization errors. In PM gyroscopes, polarization errors were minimized by minimization of polarization cross-coupling thanks to the use of the same birefringence axis throughout the gyro. Now, polarization cross-coupling in the loop is maximized by the depolarizers splices. As using only one birefringence axis throughout the gyro is no longer possible, the delays induced by the depolarizers can add to or subtract from the

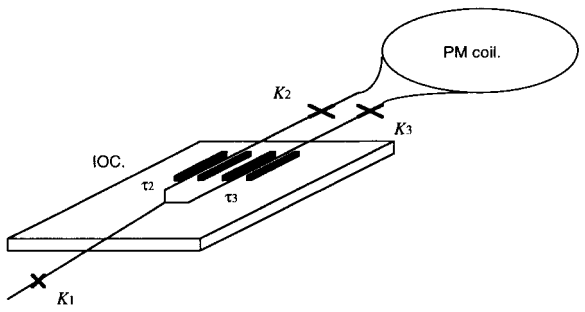


Fig. 11 PM gyro

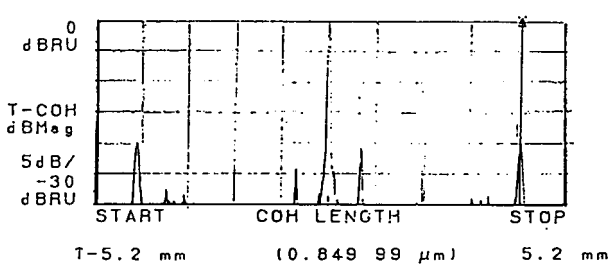


Fig. 12 A SLD's coherence function

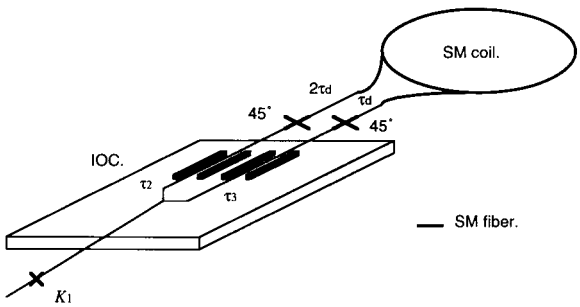


Fig. 13 Depolarized gyro

delays induced in the front end of the gyro. The coil itself has some linear and circular birefringence as a consequence of fiber bending, twisting and stresses induced within the coil. This birefringence can also add to or subtract from these delays. However, the coil birefringence is not large enough to decorrelate the waves propagating through the coil.

The way all these delays combine depends to a large degree on the evolution of the polarization within the SM coil. Consequently, error terms involve all possible combinations and change with time as polarization evolves in unpredictable ways; the same bias performance as PM gyros cannot be achieved with depolarized gyros.

## 3. LIMITATIONS

### 3.1 Transience-related effects

Even when single mode and single polarization state are used, the accuracy of an I-FOG can be limited by thermally induced non-reciprocities in the fiber coil.

Indeed, the reciprocity of the two counter-propagating paths is insured only if the system is time-invariant. Time-dependent perturbations, such as fluctuations in temperature, vibrations or acoustic noise may lead to non-negligible errors.

Thermally induced non-reciprocity was analyzed by Shupe. Thermally induced non-reciprocity can occur if there is a time-dependent temperature gradient along the fiber. Non-reciprocity arises when the corresponding wave fronts of the two counter-rotating beams traverse the same region of the fiber at different times. If the fiber's propagation constant varies at different rates along the fiber, the corresponding wave fronts in the two counter-rotating beams traverse a slightly different effective path. This creates a relatively large non-reciprocal phase shift that is indistinguishable from the Sagnac induced phase shift.

The spurious phase shift occurring in an elementary fiber segment is given by:

$$\phi_{dl} = \frac{2\pi}{\lambda}\left(\frac{dn}{dT} + n\alpha\right) \cdot dl \cdot \frac{dT}{dt} \cdot \frac{2l - L}{c} \tag{16}$$

where $n$ is the index of the fiber, $\alpha$ is the linear expansion coefficient, $c$ is the wave velocity, $L$ is the fiber length and $l$ represents the distance of the infinitesimal area from one end of the coil. We can consider that the main perturbation comes from the index change $dn/dT$.

Similar spurious phase shift is produced by time-dependent mechanical stresses. For example, a sinusoidal vibration on an elementary segment of the fiber $dl$ causes an error given by:

$$\phi_{dl} = \frac{2\pi}{\lambda}\left(\frac{dn}{d\sigma} + \frac{n}{ES}\right) \cdot dl \cdot \frac{d\sigma}{dt} \cdot \frac{2l - L}{c} \tag{17}$$

$$\sigma = \sigma_0 \sin \omega t$$

where $\omega$ is the angular frequency of vibration, $E$ is the Young's modulus, $S$ is the sectional area of the fiber. When this periodic vibration is sufficiently rapid compared to the time constant of the I-FOG signal processing, no bias drift arises. If the variation is slower than the time constant, a drift is generated and a noise appears at the output of the gyro. This error is considered to be produced by oscillation of the fiber inside the coil, oscillation of the leads and mechanical resonance of the structural parts.

The optical power can also vary being synchronized with the period of vibration. This periodic variation of the optical power is usually due to periodic changes in alignment of the fibers with the light source module and the IOC. An additional bias drift is yielded by this synchronous variation of optical power.

To overcome these problems, several winding configurations of the sensing coil have been proposed. Compensation of time-dependent perturbations is obtained by a symmetrical winding where symmetrical segments are closely placed. The so-called dipolar winding reduces the effect of thermal transience by a factor approximately equal to the number of layers. The quadrupolar winding is a more complex but even better compensation method. The effect of thermal transience is reduced by the square of the number of layers.

An adequate potting has to be used to ensure the coil ruggedness and securing the winding by impregnation with varnish is an efficient technique for preventing the oscillations of the fiber inside the coil. An adequate mechanical design is also required to set up the mechanical resonance point far from the perturbation frequency range.

Finally, the use of optical components with environmental ruggedness reduces the periodic change in optical power and thereby, prevents from bias drift.

### 3.2 Backreflection and backscattering

The 4% Fresnel backreflection at the air-silica interface of the fiber coil ends surimposes a parasitic Michelson interferometer. As antireflection coating cannot provide a low enough level of backreflected light, the solution is still to polish the fiber ends at a sufficient slant angle and to align them according to refraction laws so as not to degrade the coupling. Once these spurious reflected waves are reduced, a low coherence source destroys the coherence between the primary waves and these spurious waves, avoiding direct coherent detection.

Rayleigh backscattering preserves the same optical frequency as the primary wave and can be considered as a randomly distributed backreflection due to inhomogeneities in the fiber. Rayleigh scattering is caused by dipolar antenna radiation of the material atomic bindings excited by the incoming wave. Scattered radiation produces a secondary pair of waves propagating in the fiber. The forward scattering is reciprocal and does not yield any spurious effect in the fiber gyro. On the contrary, the backward scattering behaves like a randomly distributed backreflection and yields a spurious phase difference because of the coherent detection process with the primary wave acting as a local oscillator. The low coherence length of a broad-band source preferably used in an I-FOG decreases considerably the Rayleigh backscattering noise.

### 3.3 Truly non-reciprocal effects

Even in a perfectly reciprocal system, the Sagnac effect is not the only truly non-reciprocal effect.

The Kerr effect manifests itself as intensity-dependent perturbations of the fiber's propagation constant. Reciprocity is indeed based on the linearity of propagation equation, but an imbalance in the power levels of the counter-propagating waves can produce propagation non-linearity because of the high optical power density in the very small silica fiber core. Therefore, the Kerr effect yields a spurious non-reciprocal phase difference. It could be reduced by simply reducing the power in the fiber, but this would relatively increase the influence of detection noise. Concerning the Kerr effect too, the use of a broad-band light source is a simple and efficient solution.

It has been reported that an I-FOG used under the earth's magnetic field shows a drift nearly equal to the earth rotation rate, caused by the Faraday effect. When an I-FOG is located in a magnetic field, its fiber loop acts as a Faraday device and the polarization plane of the linearly polarized wave in the fiber rotates. If the sensing loop is made of ideal circular single-mode fiber, the Faraday effect is canceled while the light travels once in the fiber loop and no spurious phase difference is generated. However, in a practical fiber, a phase difference appears due to polarization changes along the fiber arising from residual birefringence. The use of PM fiber reduces the magnetic dependence.

## 4. ERRORS

At rest, the output signal of an I-FOG is composed of a white noise and a slowly varying function representing the long-term drift of the mean value.

### 4.1 Drift

Drift corresponds to the residual lack of reciprocity in the I-FOG, usually expressed in ± °/h. As described in the previous chapters, the different causes of drift can be:

- a limited spatial rejection of the single-mode filter.
- a limited polarization control.
- a time-dependent temperature gradient.
- Faraday effect.
- Kerr effect.
- defects in the modulation or demodulation processes.

### 4.2 Noise

In an I-FOG, the theoretical noise limit is the detection noise. Different units are used to evaluate the white noise:

- standard deviation of equivalent rotation rate per square root of bandwidth of detection or $(\mathrm{deg}/h)/\sqrt{Hz}$.
- equivalent noise power spectral density or $(\mathrm{deg}/h)^2/Hz$.
- random walk performance or $\mathrm{deg}/\sqrt{h}$.

As described in the previous chapters, the different causes of noise are:

- Rayleigh backscattering.
- time-dependent mechanical stresses.
- detection noise.

### 4.3 Noise/Drift

Noise and drift correspond to different requirements which depend on the applications. If a fast stabilization and control response is required, then noise is important, but, for navigation, drift is the fundamental parameter. In navigation applications, the angular orientation is calculated by integrating the rotation rate signal. This process of integration inreases the effect of averaging the white noise and, consequently, makes the drift in the long term dominant .

### 4.4 Scale factor

Major advantages of the I-FOG technology are that it offers the potential of a low-cost, all solid-state approach with long-lifetime and high-reliability over current gyros. In order to fully exercise these advantages, it is imperative that these gyros have scale factors compatible with strapdown applications. An accurate scale factor is necessary to have an accurate measurement of high rates and so, the scale factor stability and the scale factor linearity are very important characteristics of the gyro. Closed-loop modulation is an efficient solution to achieve higher dynamic range and high scale factor accuracy. The scale factor stability depends on the stability of both the wavelength and the equivalent area of the coil.

## 5. RECAPITULATION OF THE THEORETICAL PART

### 5.1 Optimal operating conditions

- Polarization effects.
- Non-ideal polarizers.
- Non-ideal modulators.
- Presence of higher order modes.
- Time-dependent temperature gradient.
- Mechanical stress induced effects.
- Scattering from interfaces.
- Rayleigh backscattering.
- Kerr effect.
- Faraday effect.
- Light source problems.
- Etc.

The above lists several error sources that must be dealt with in order to achieve good performance. To overcome these problems, optimal operating conditions can be established :

- a single-mode reciprocal configuration using a single spatial-mode and single polarization-mode filter at the common input-output port of the interferometer.
- a modulation biasing scheme with a reciprocal phase modulator within the sensing coil.
- a broad-band light source with a short coherence length.
- PM fiber.
- a closed-loop configuration operating the interferometer at null.
- wavelength control.

### 5.2 State of art

After 20 years of research and development, the I-FOG is now recognized as a crucial technology for many applications of inertial guidance and navigation. Even though high grade gyros for space applications are still under development, some moderate grade commercial gyros are already mass-produced. The prospect that I-FOG would replace mechanical and ring laser gyroscopes in many applications has traditionally been the motivation for continuing development of I-FOG technology. The main advantages of I-FOG are : low-mass solid-state configuration, long lifetime, high reliability, high dynamic range, ability to withstand shocks and vibrations, large bandwidth, nearly instantaneous start-up and low power consumption. The main applications now deal with intermediate grade gyros (0.1 to 10°/h) : Attitude and Heading Reference Systems for airplanes and helicopters, bore-hole survey, robotics, car navigation systems aided by GPS. As some of these markets are exceedingly price sensitive, it has been questioned whether an I-FOG can be produced to satisfy the technical and price requirements and this was the main thread of the experimental part of our research.

## 6. EXPERIMENTS OF I-FOG DERIVED FROM JG-108FA

### 6.1 Performance and applications

An I-FOG can achieve various performance levels according to its configuration: open- or closed-loop, fiber length, signal processing, etc. Consequently, the I-FOG technology has a wide field of applications that can be divided into three main grades : inertial, intermediate and moderate as shown in Table 1.

JG-108 FA, made by JAE Ltd., is a moderate grade gyro with analog output. Its performance can be defined as :

- Bias drift: 0.1 °/s max.
- Scale factor stability :± 3 %.
- Scale factor linearity :± 1 %FS (% per full scale) max.
- Temperature range : from − 20 °C to +70 °C.
- Dynamic range :± 100 °/s.
- Sinusoidal vibration : 5G, 20 to 200 Hz.
- Shock: 40 G, 11ms.

This low-cost moderate grade gyro is mainly used for angu-

Table 1 Main grades of I-Fog.

| | Noise | Bias drift (1σ value) | Scale factor accuracy (1σ value) |
|---|---|---|---|
| Inertial grade | <0.001 °/$\sqrt{h}$ | <0.01 °/h | <5 ppm |
| Intermediate grade | 0.5 to 0.05 °/$\sqrt{h}$ | 0.1 to 10 °/h | 10 to 1000 ppm |
| Moderate grade | >0.5 °/$\sqrt{h}$ | 10 to 1000 °/h | 0.1 to 1 % |

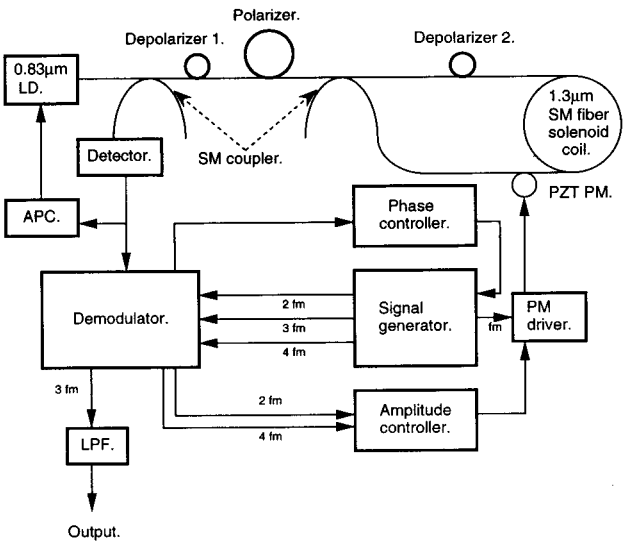


Fig. 14 Configuration of JG-108 FA

lar rate measurements in commercial applications: camera stabilizer, auto-guided tractor, guidance and control for R/C helicopter.

A digital output version of JG-108 FA exists and is commercialized as JG-108 FD.

### 6.2 Configuration

Fig. 14 shows the configuration of JG-108 FA. The required dynamic range is not so wide, so an open-loop modulation has been adopted. JG-108 FA is an all-fiber gyro with a Laser Diode as light source and a PZT phase modulator.

All-fiber approach serves to simplify and to stabilize the system. It eliminates the problem of tight alignment tolerances and provides simplicity and packageability. All-fiber approach usually provides very good signal-to-noise ratio and bias performance, but the scale factor accuracy is limited in practice to about 0.1%. To improve the scale factor, optical power level at the detector, amplitude of phase modulation and phase difference at the demodulator are carefully controlled by the open-loop signal processing circuit.

In this configuration of gyro, the production cost is mainly raised by the working time necessary for 10 splicing points and also by the cost of polarizer and depolarizers. If the splicing points can not be suppressed in such an all-fiber approach, we will study the real influence of polarizer and depolarizers in order to propose a lower cost configuration of JG-108 FA for mass production.

### 6.3 Components

(1) Light source

The main requirements for the light source are good spatial coherence, low temporal coherence, sufficient output power to achieve high performance. Depolarized gyros especially require a lower coherence function of the light source. A LD provides a spatially coherent light but its spectrum is composed of narrow emission peaks due to the Fabry-Perot modes of the Laser cavity. To reduce this temporal coherence, the LD should be driven below threshold current but this reduces the output power and so, increases the RIN (relative intesity noise). Another solution simultaneously to get a good spatial coherence and a low temporal one is to use Super Luminescent Diodes (SLD) in which the Laser effect is suppressed. The gain of these diodes is very high, even without cavity effect. The first spontaneous emission photons are amplified by stimulated emission. The output wave is generated in a narrow stripe and so, has a spatial coherence similar to the one of a LD. Fig. 15 shows the coherence functions of LD and SLD measured at T = 25°C.

Even if the LD is operated below threshold, its temporal coherence is higher than the SLD's one; its second peaks due to the Fabry-Perot modes are closer to the main peak and of higher amplitude. Moreover, as regards to the production cost and to the output power level too, present SLD technology seems to be the appropriate choice for this gyro configuration. Nevertheless, for the construction of our engineering model of JG-108 FA, we used a 0.83$\mu$m pulsation type LD. This LD fits the SM fiber for 1.3$\mu$m used in the sensing coil and is now on mass production as a key component of compact disc technology. As the characteristics of a SLD would be more appropriated to our application, the results we will get with the engineering model will represent the worst case of performance.

In such a depolarized gyro, we can expect the limitation of polarization control to be the main error source. Therefore, to

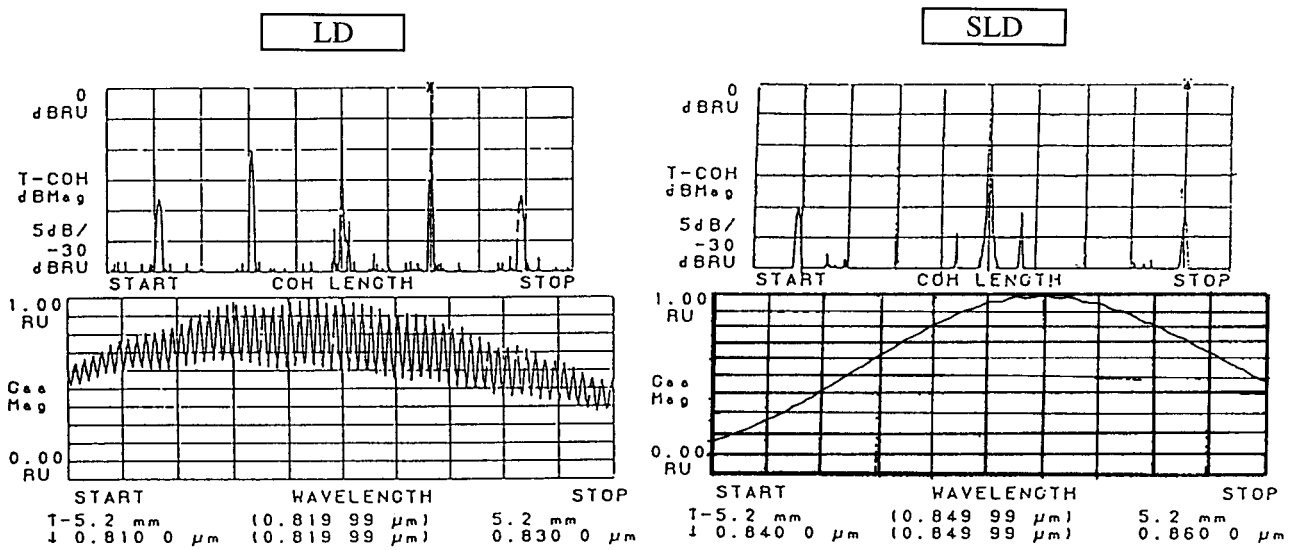


Fig. 15 Coherence functions of LD and SLD

analyze the LD influence in this I-FOG configuration, we must first evaluate its coherence function.

On the one hand, the coherence function of the LD increases with the drive current since higher drive current leads to higher LD efficiency and so, higher Laser effect (cf. Fig. 16). On the other hand, by reducing the drive current, we reduce the output optical power and then increase the RIN. A compromise has to be found between RIN and bias drift caused by high coherence function.

The LD's coherence function also depends on the temperature (cf. Fig. 17). For a given optical power, when the temperature increases, the LD efficiency decreases because of semiconductor characteristics and then the temporal coherence of the light source is reduced.

To achieve simultaneously low bias drift and low RIN, the LD is driven by an APC (Automatic Power Control) circuit to be operated with a power level of 0.25$\mu$W at the detector but, as it is low cost configuration, no temperature compensation is necessary.

The LD influence also depends on its wavelength stability. The emitted wavelength varies with the temperature and the LD's drive current. Wavelength instability generates variations of scale factor. Using an APC circuit and no temperature compensation, this configuration cannot reach a high scale factor stability.

Finally, another important characteristic of the light source may be the polarization state of the emitted light. The LD we

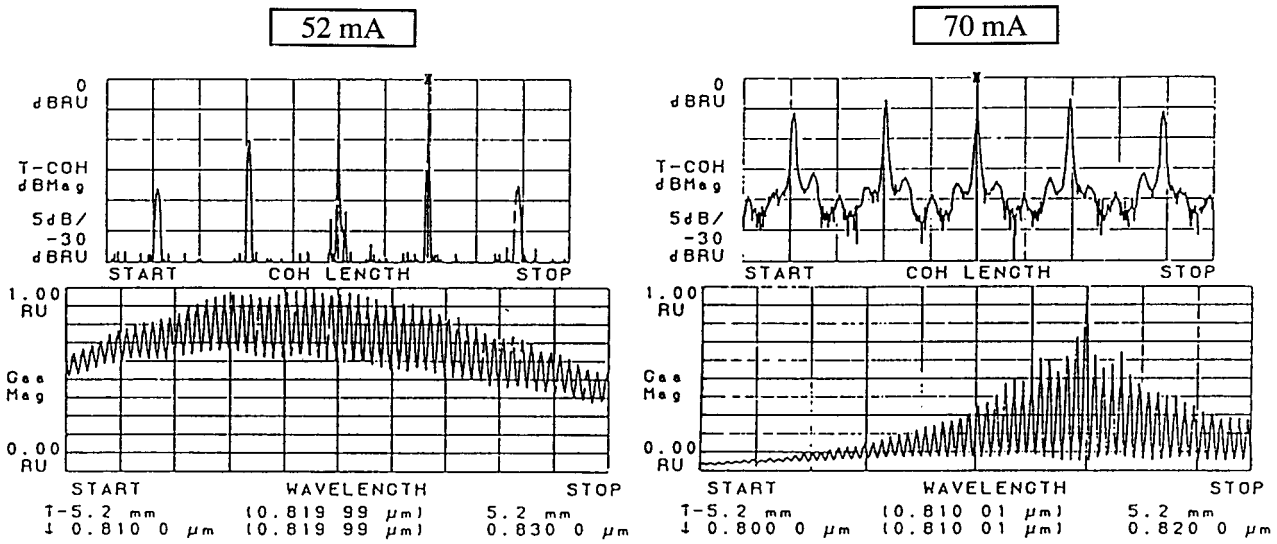


Fig. 16 Influence of the drive current on the coherence
(function: $I_f$ = 52mA and $I_f$ = 70mA for T = 25°C.)

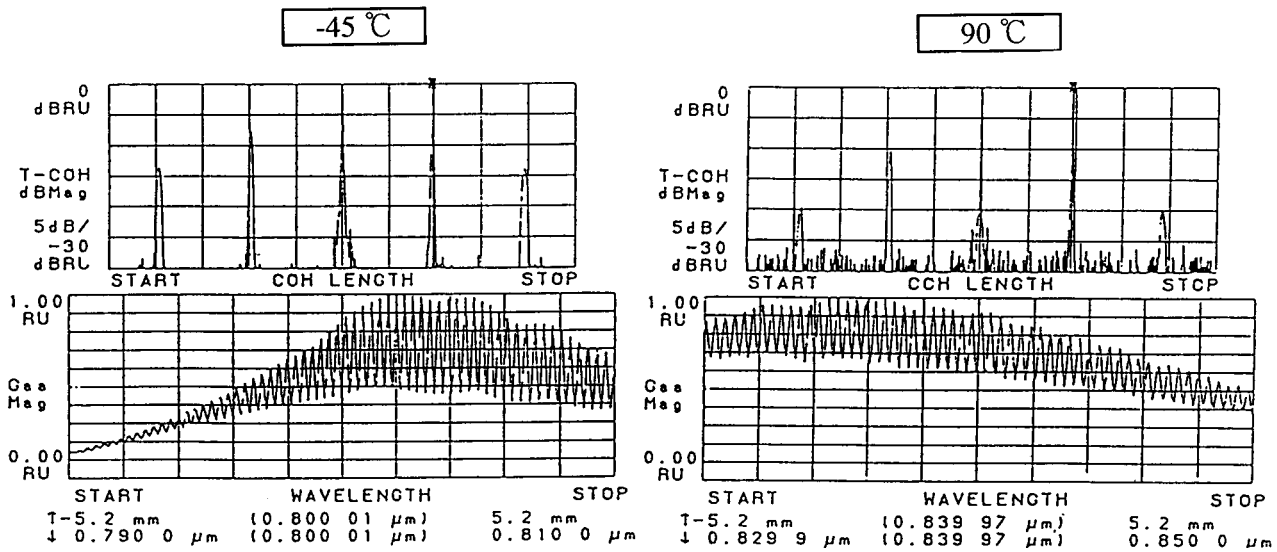


Fig. 17 Influence of the temperature on the coherence
(function: T = − 45°C and T = 90°C for $I_f$ = 46*mA*.)

used has a polarization degree P = 0.3 when $I_f$ whereas present SLD modules could easily provide a split power between the two orthogonal axes (P<0.3).

(2) Sensing coil

The fiber coil is made out of 180m of SM fiber for 1.3$\mu$m with a cladding diameter of 125$\mu$m, that is to say superior to the standard diameter of gyro fibers, 80$\mu$m. This SM fiber does not allow to achieve the same performance as PM gyros and tends to increase the volume of the sensing coil. Nevertheless, it meets the requirements of moderate grade gyros and, what is more, mass production for optical communications makes SM fiber a low cost component.

The diameter of the coil is 61.5mm and the winding is conventional solenoid technique instead of quadruple technique. This conventional technique is less effective to reduce thermally induced non reciprocities but results in a shorter working time and, consequently, in a lower production cost.

Finally, the problem caused by the recorrelation peaks of the LD's coherence function is not only solved by placing a SM filter between the couplers but also by bending the fiber. In that case, the cut off frequency of the fiber decreases and only the fundamental mode can be transmitted.

(3) Heart of the interferometer

It consists of two SM couplers, two depolarizers, a polarizer and a PZT phase modulator associated in an all-fiber approach. The source coupler and the coil one are fused taped couplers. The depolarizers are Lyot type depolarizers made out of PANDA fiber. The fiber is cut so that the length ratio of the two parts is 2:1 and spliced again at 45°. Requirements for these depolarizers are:

- To decorrelate the two orthogonal waves with a birefringence induced delay.
- To insure even splitting of the light between the two orthogonal axes.

Lengths of depolarizers 1 and 2 are respectively 90cm and 180cm. This insures the decorrelation of the two orthogonal waves. The polarization degree P of the light is defined with the respective intensities of the polarization modes and should be null for an even splitting of intensity between the two orthogonal axes.

$$P = \frac{I_x - I_y}{I_x + I_y}. \tag{18}$$

The polarization degree of the light at the output of the depolarizers varies with the splice angle accuracy and should be null for 45°. The depolarizers of the engineering model we realized are characterized by :

$P_1 = 0.048$

$P_2 = 0.045$.

The polarizer is made out of coiled PANDA fiber for polarizer. When this stress-induced high-birefringence fiber is coiled, a differential curvature loss occurs between the two polarization states and yields the rejection of one axis. The polarizer is a high cost component in our gyro configuration. The one we used has a power extinction ratio $\varepsilon^2 = -40dB$.

The PZT phase modulator is realized by winding a High-NA SM fiber around a piezoelectric tube. This type of SM fiber has very low bending losses. The tube diameter controlled by a driving voltage modifies the optical length of the fiber. The frequency modulation of the PZT modulator is about 45kHz.

The heart of the interferometer is also composed of a detector but, for moderate grade gyros, the characteristics of this component are not so critical since the gyro performance is not affected by a shot noise.

### 6.4 Tests and evaluation

(1) Method

Among the devices of the I-FOG, the interferometer, especially a depolarizer and a polarizer, costs a great deal because splicing two fibers requires a time-consuming job. The aim of our survey is to evaluate the influence of the two depolarizers and of the polarizer on the gyro performance. Therefore, we studied the gyro performance in four different cases of optical configuration.

Table 2 Set if rates

| CW ( °/s ) | CCW ( °/s ) |
|---|---|
| 10 | 10 |
| 20 | 20 |
| 30 | 30 |
| 40 | 40 |
| 50 | 50 |
| 60 | 60 |
| 70 | 70 |
| 80 | 80 |
| 90 | 90 |
| 100 | 100 |

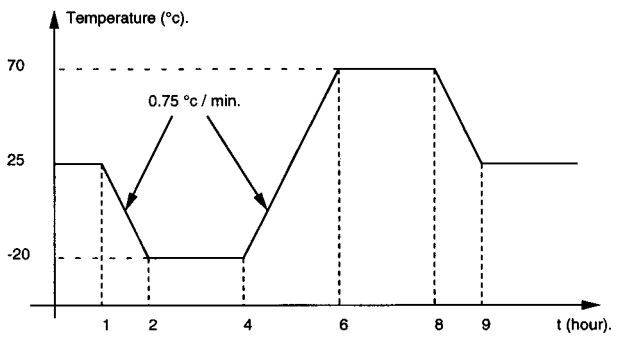


Fig. 18 Thermal cycle

The first case was the general configuration and then, we removed successively depolarizer 1, depolarizer 2 and the polarizer.

For each case, we measured the performance mainly in terms of bias drift, scale factor and noise. Scale factor tests were performed at 25 ˚C, − 20˚C and 70˚C by rotating the rate table through the set of fixed rates shown by Table 2. Bias stability tests were performed in a thermal chamber by applying the thermal cycle described by Fig. 18. No input rotation rate was applied and a 5Hz low-pass filter was used to eliminate major part of the short term fluctuations. During these tests, we also measured the power level at the detector, the LD's drive current and other significant voltage levels in the electronic circuit to estimate the efficiency of the feedback loop. Noise represents short term instability. It was studied by measuring the spectrum of the gyro output without applying rotation rate, on a special support reducing vibrations. So, this measurement is composed of the electronic noise of the circuit and of the optical noise for the gyro at rest under stable temperature. The frequency range of measurement was from 1Hz to 1kHz.

No tests for bias stability and noise under vibration were performed on this engineering model since the components were not properly fixed.

Before each succession of tests, we measured the output power level for the optical part of the gyro for a drive current $I_f = 46mA$ (corresponding to P = 0.25$\mu$W without modulation in the general configuration) and checked its stability when the SM fiber from the coil or from the LD was bent. In that way, we could observe the influence of the depolarizers and of the polarizer on the optical power level and its stability. Then, we adjusted the feedback circuit and measured the LD's drive current. This drive current has a low limitation and a high one respectively due to the LD and to the feedback circuit.

(2) First case

First, we measured the performance of the general configuration of JG-108 FA (cf. Fig. 14) as reference for other cases.

The requirements for the scale factor are:

- temperature stability: ± 3%.
- linearity error: ± 1%FS.

This first configuration meets the scale factor requirements (cf. Table 3 and Fig. 19).

During bias test, we measured the LD's drive current. It varied from 37mA at − 20˚C to 61mA at 70˚C. This variation yields a wavelength change (cf. Fig. 20) which is the main cause of the scale factor temperature instability. This variation of scale factor can be evaluated by:

$$\Delta SF(T, T_0) = \frac{\dfrac{1}{\lambda(T)} - \dfrac{1}{\lambda(T_0)}}{\dfrac{1}{\lambda(T)}} \qquad (19)$$

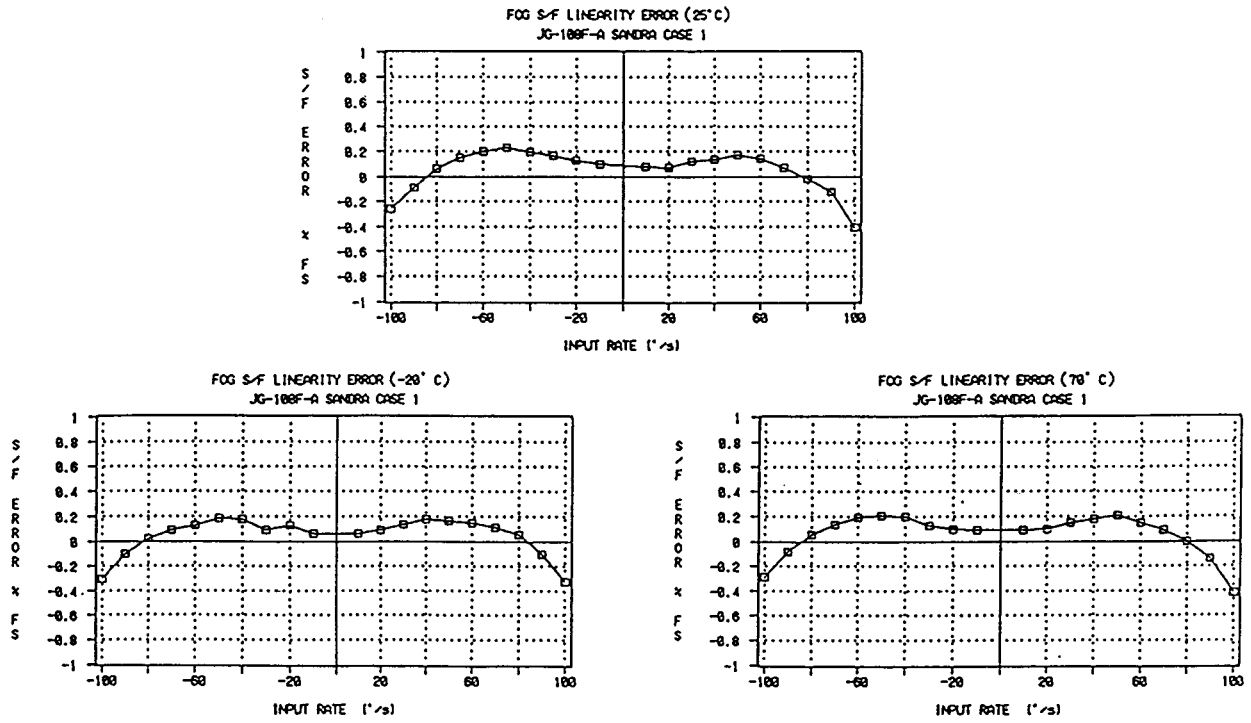


Fig. 19 Scale factor linearity error: case 1

Table 3 Scal factor test data: case 1

JG-108FA SCALE FACTOR ANALYSIS

| | | | |
|---|---|---|---|
| Assy No. | SANDRA | DATE | '96/06/25 |
| Serial No. | CASE 1 | | |
| OPTICALSENSOR Assy No. | SANDRA | FIBER LENGTH | 180m |
| SENSOR ELEC Assy No. | CASE 1 | | |

| INPUT RATE[°/s] | +25℃ OUTPUT(V) | | −20℃ OUTPUT(V) | | +70℃ OUTPUT(V) | |
|---|---|---|---|---|---|---|
| -100 | -4.791 | | -4.861 | | -4.695 | |
| -90 | -4.320 | | -4.384 | | -4.235 | |
| -80 | -3.848 | | -3.903 | | -3.772 | |
| -70 | -3.373 | | -3.420 | | -3.306 | |
| -60 | -2.896 | | -2.935 | | -2.839 | |
| -50 | -2.418 | | -2.451 | | -2.370 | |
| -40 | -1.937 | | -1.964 | | -1.900 | |
| -30 | -1.456 | | -1.473 | | -1.427 | |
| -20 | -0.975 | | -0.988 | | -0.956 | |
| -10 | -0.494 | | -0.498 | | -0.486 | |
| 10 | 0.473 | | 0.482 | | 0.462 | |
| 20 | 0.952 | | 0.970 | | 0.932 | |
| 30 | 1.434 | | 1.459 | | 1.404 | |
| 40 | 1.914 | | 1.948 | | 1.875 | |
| 50 | 2.395 | | 2.434 | | 2.346 | |
| 60 | 2.873 | | 2.920 | | 2.813 | |
| 70 | 3.349 | | 3.405 | | 3.280 | |
| 80 | 3.824 | | 3.889 | | 3.745 | |
| 90 | 4.298 | | 4.368 | | 4.208 | |
| 100 | 4.764 | | 4.844 | | 4.665 | |
| | | | | | | |
| OFFSET(V) | -0.010 | | -0.008 | | -0.012 | |
| | 0.04794 | | 0.04868 | | 0.04697 | |
| SCALE FACTOR (mV/°/s) | 47.937 | | 48.678 | | 46.965 | |
| TEMPERATURE STAB (±3%) [%] (related to 25℃) | 0.0000 | | 1.5464 | | -2.0270 | |
| LINEARITY ERROR(±1%) [%/FS] | 0.2324 | MAX | 0.1865 | MAX | 0.2071 | MAX |
| | -0.4113 | MIN | -0.3255 | MIN | -0.4162 | MIN |

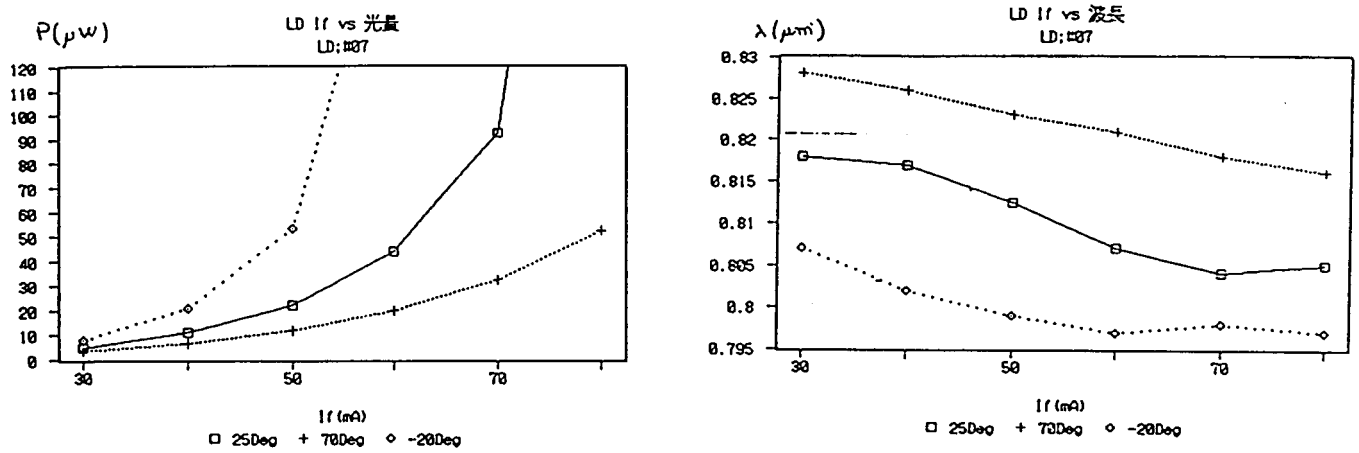


Fig. 20 LD's characteristics: P = f($I_f$) and $\lambda$ = f($I_f$)

Table 4 $\lambda$-depence of scale factor stability

| | 25°c | -20°c | 70°c |
|---|---|---|---|
| If (mA) | 46 | 37 | 61 |
| $\lambda$ ($\mu m$) | 0.814 | 0.803 | 0.821 |
| $1/\lambda$ | 1.2285012285 | 1.2453300125 | 1.2180267966 |
| $\Delta SF(T,25°c)$ | 0 | +1.37% | -0.85% |

Using the data from Fig. 20, we can estimate that, if the scale factor depends only on the wavelength, in the best case, we can achieve a scale factor stability of about ± 1.37% (cf. Table 4).

The comparison between Table 3 and Table 4 indicates that the scale factor temperature stability is actually in the order of the scale factor variation caused by the wavelength change. Nevertheless, the scale factor does not depend only on the light source wavelength. It may be influenced by a change of the coil area due

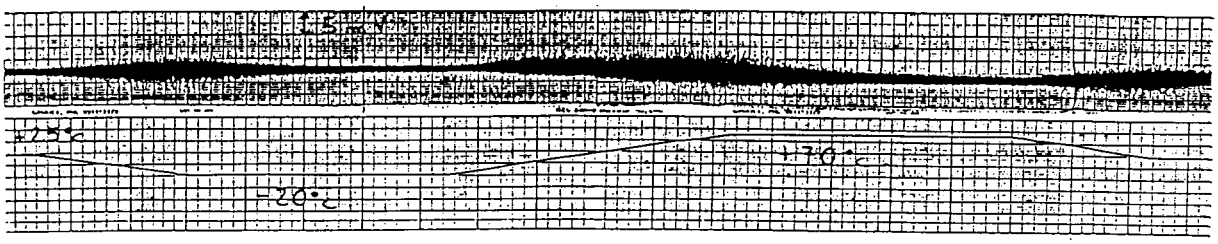


Fig. 21 Bias test data: case 1

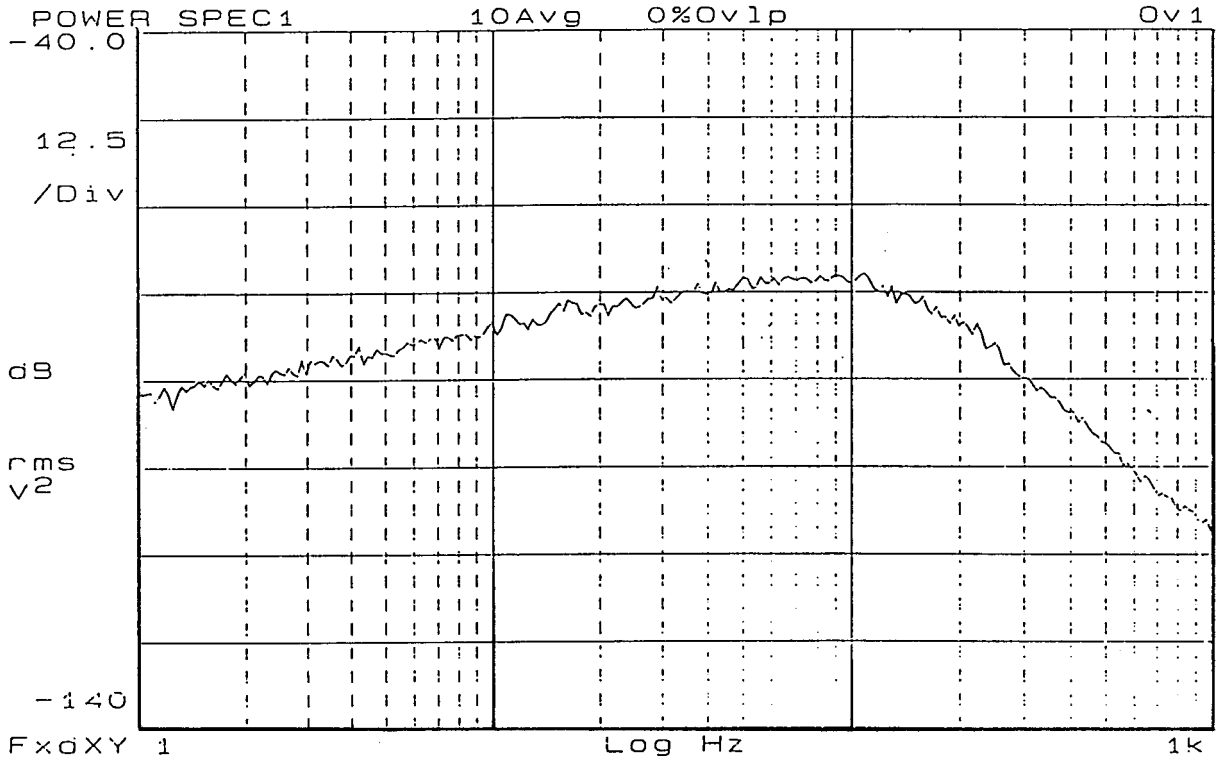


Fig. 22 Spectrum of the gyro's output: case 1

to temperature variation and also by the feedback loop performance, that is to say, stabilities of the output power level, the phase modulation amplitude and the phase shift at the demodulator. As regards to that point, we can notice in Fig. 20 (left) that the gain of the APC loop is higher for − 20°C than for 70°C and this may explain why the scale factor temperature stability is better for − 20°C than for 70°C.

The bias drift observed over the thermal cycle was 0.03°/s. This value meets the requirements of JG-108 FA as the bias drift less than 0.1°/s (cf. Fig. 21).

Fig. 22 shows the spectrum of the gyro output measured on a vibration reducing table without applying rotation rate. These measurements are not used to check the noise requirements since they don't take into account the vibrations of the gyro under normal operating conditions, but we shall use them to compare the noise characteristics in the four different configurations. In this first case, we can already notice a 100Hz low-pass filter in the electronic circuit.

Table 5 should be used to translate the gyro noise from dB to °/s peak to peak in figures 22, 27 and 30 and the gyro noise from dB to V in figures 22, 23, 27 and 30.

Table 5 Gyro noise translation table

| Noise (dB) | Noise (V) | Noise (°/s pp) |
|---|---|---|
| -40.0 | 1.0000E-02 | 2.0861E-01 |
| -52.5 | 2.3714E-03 | 4.9469E-02 |
| -65.0 | 5.6234E-04 | 1.1731E-02 |
| -77.5 | 1.3335E-04 | 2.7818E-03 |
| -90.0 | 3.1623E-05 | 6.5967E-04 |
| -102.5 | 7.4989E-06 | 1.5643E-04 |
| -115.0 | 1.7783E-06 | 3.7096E-05 |
| -127.5 | 4.2170E-07 | 8.7969E-06 |
| -140.0 | 1.0000E-07 | 2.0861E-06 |

Figures 23 and 24 represent respectively the electronic noise of the gyro and the noise of the measurement equipment. So, we can assume that, in the general configuration at rest, major part of the noise is not optical noise.

We can check the noise requirements on the data taken during bias test and confirm that this gyro presents a noise less than 0.04°/s for f < 5Hz at rest and under stable temperature (production requirements : noise inferior to 0.08°/s with 5 Hz low-pass

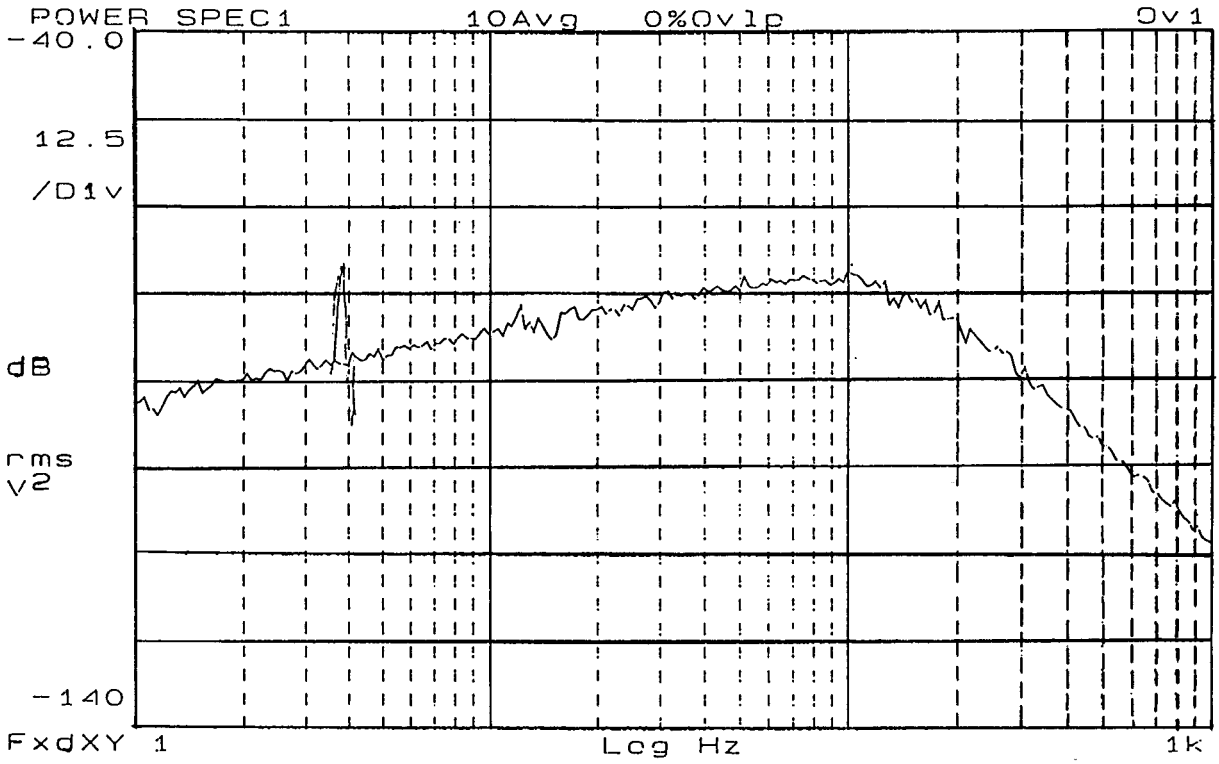


Fig. 23 Electronic noise

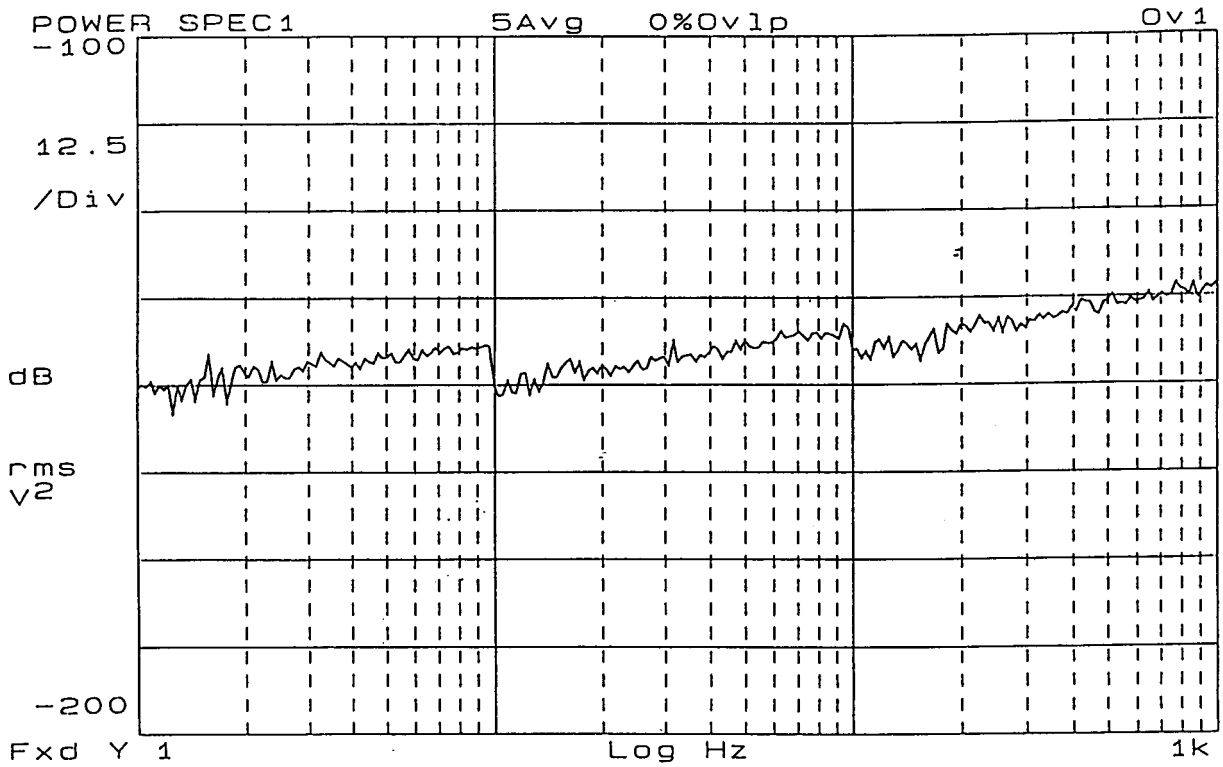


Fig. 24 Noise of the measurement equipment

filter, gyro at rest and under stable temperature).

After the assembling of the gyro optical part, we measured the optical output power P = 0.22$\mu$W when $I_f$ = 46mA and checked that this power was constant when the SM fiber from the coil or from the LD was bent. After the adjustment of the feedback circuit, the drive current was 45.8 mA.

(3) Second case

For this second case, we removed depolarizer 1 (cf. Fig. 25). The polarization degree of the light emitted by the LD for $I_f$ = 46

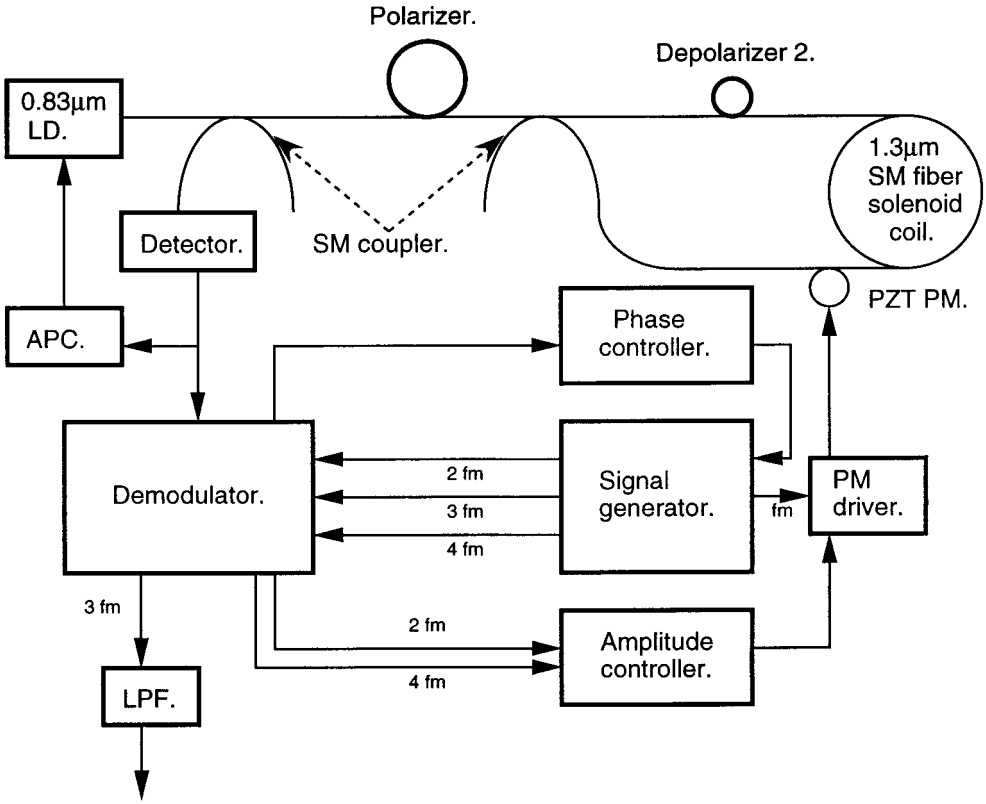


Fig. 25 Second configuration

Table 6 Scale factor test data: case 2

JG-108FA SCALE FACTOR ANALYSIS

| | | | |
|---|---|---|---|
| Assy No. | SANDRA | DATE | '96/06/25 |
| Serial No. | CASE 2 | | |
| OPTICALSENSOR Assy No. | SANDRA | FIBER LENGTH | 180m |
| SENSOR ELEC Assy No. | CASE 2 | | |

| INPUT RATE[°/s] | +25℃ OUTPUT[V] | | −20℃ OUTPUT[V] | | +70℃ OUTPUT[V] | |
|---|---|---|---|---|---|---|
| -100 | -4.784 | | -4.867 | | -4.678 | |
| -90 | -4.315 | | -4.389 | | -4.222 | |
| -80 | -3.842 | | -3.909 | | -3.761 | |
| -70 | -3.367 | | -3.425 | | -3.298 | |
| -60 | -2.891 | | -2.940 | | -2.833 | |
| -50 | -2.414 | | -2.454 | | -2.364 | |
| -40 | -1.934 | | -1.965 | | -1.897 | |
| -30 | -1.455 | | -1.478 | | -1.429 | |
| -20 | -0.975 | | -0.987 | | -0.959 | |
| -10 | -0.492 | | -0.498 | | -0.491 | |
| 10 | 0.471 | | 0.483 | | 0.451 | |
| 20 | 0.951 | | 0.974 | | 0.920 | |
| 30 | 1.433 | | 1.462 | | 1.391 | |
| 40 | 1.912 | | 1.943 | | 1.859 | |
| 50 | 2.391 | | 2.440 | | 2.327 | |
| 60 | 2.869 | | 2.928 | | 2.794 | |
| 70 | 3.345 | | 3.410 | | 3.259 | |
| 80 | 3.820 | | 3.897 | | 3.723 | |
| 90 | 4.291 | | 4.378 | | 4.182 | |
| 100 | 4.764 | | 4.856 | | 4.640 | |
| | | | | | | |
| OFFSET(V) | -0.012 | | -0.007 | | -0.020 | |
| | 0.04788 | | 0.04876 | | 0.04675 | |
| SCALE FACTOR (mV/°/s) | 47.878 | | 48.761 | | 46.752 | |
| TEMPERATURE STAB (±3%) [%] (related to 25℃) | 0.0000 | | 1.8437 | | -2.3528 | |
| LINEARITY ERROR(±1%) [%/FS] | 0.1899<br>-0.3304 | MAX<br>MIN | 0.1917<br>-0.3300 | MAX<br>MIN | 0.2014<br>-0.3672 | MAX<br>MIN |

mA is P = 0.3 which corresponds to a power ratio between the orthogonal axis equal to 2:1 and, when passing through SM fiber, this light may undergo unpredictable evolution. This polarization evolution of the light entering the polarizer yields variations of the optical power and may even generate signal fading. The role of depolarizer 1 was to provide depolarized light to the polarizer's input, that is to say, to avoid signal fading and to stabilize the optical power. Nevertheless, concerning optical power stabilization, we must notice that the APC circuit is already used and so, depolarizer 1 is only necessary to avoid large variations of optical power.

For this second case, scale factor temperature stability and linearity error are quite similar to those measured for the first case and they meet the requirements of JG-108 FA (cf. Table 6). As a matter of fact, the drive current increase from 36mA at −20°C to 72mA at 70°C and the correct operation of the feedback loop should have generated a scale factor temperature stability equivalent to the one in the first case. The scale factor stability is slightly better in the general configuration but this result may be explained by the imprecision of the rate table. To make sure that this result needs to be explained, we should have performed repeatability tests that are not required for moderate grade gyros. Anyway, this result confirms that depolarizer 1 is not so useful to achieve a stable power level.

The bias drift in this second configuration is 0.02 °/s, even slightly better than for the first case (cf. Fig. 26). This result confirms that depolarizer 1 is not useful for polarization error control.

Fig. 27 represents the noise at the gyro output. By comparing figures 22 and 27, we can notice that the removal of depolarizer 1 does not yield any additional output noise. Nevertheless, an in-depth survey of this gyro performance should perform vibration tests and, at that time, we might observe additional noise for the second configuration. Finally, the data taken during bias test

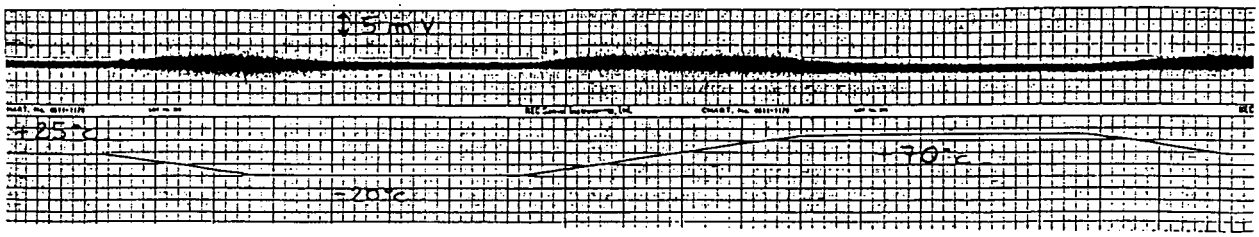


Fig. 26 Bias test data: case 2

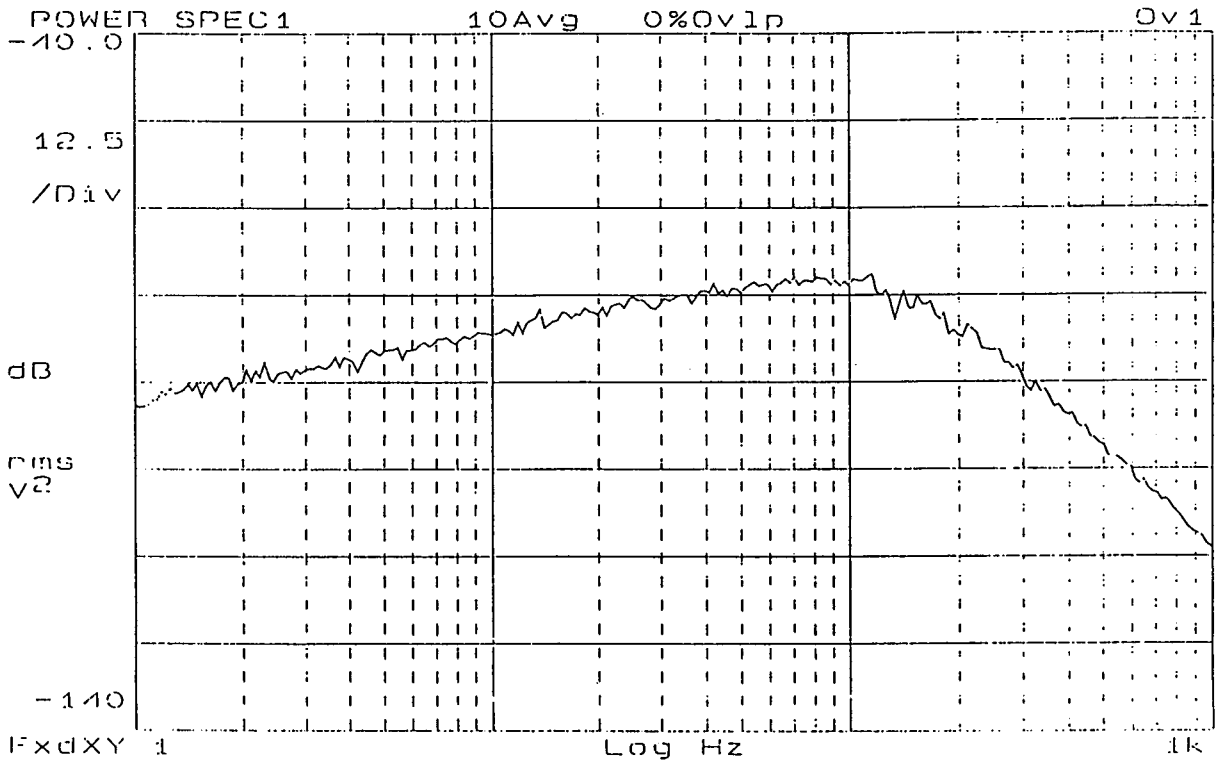


Fig. 27 Spectrum of the gyro's output: case 2

confirm that this configuration meets the noise requirements of JG-108 FA.

After the assembling of the gyro's optical part, we measured the optical output power P = 0.248$\mu$W when $I_f$ = 46mA. This output power is a little bit higher than for the first case. It slightly varies when the SM fiber from the LD is bent but we did not observe signal fading. So, the removal of depolarizer 1 did not yield so significant power fluctuations; the polarization degree of the light reaching the polarizer is not so high. After the adjustment of the feedback circuit, the drive current was 43.1 mA, so the operating point of the feedback loop was quite similar to the general configuration one.

(4) Third case

For this third case, we removed depolarizer 2 (cf. Fig. 28). The polarization state of the light entering the coil is linear and it may undergo unpredictable evolution when passing through SM fiber. This polarization evolution within the coil generates polarization errors and fluctuations of the power level at the detector. The role of depolarizer 2 was to provide depolarized light to the coil.

The scale factor linearity error still meets the requirements of JG-108 FA but the scale factor temperature stability was deteriorated in this third case (cf. Table 7). We can check that this degradation is not due to the wavelength change but to the feedback circuit that does not manage to exactly compensate the effects of polarization variations. As a matter of fact, the feedback loop was not able to insure stable power level at the detector and phase matching between detected signal and reference at the demodulator. In this open-loop configuration, the scale factor varies linearly with the power level. So, we can guess that this instability is the main cause of degradation of the scale factor stability.

The bias drift is 0.63°/s and sinusoidal drift appeared during temperature ramping (cf. Fig. 29). This bias drift does not meet the requirements of JG-108 FA because the reduction of polarization control within the SM coil increased the polarization errors. This result emphasizes the necessity to feed a SM coil with a depolarized light averaging the polarization errors.

From Fig. 30, we can assume that the removal of depolarizer 2 does not generate any additional noise when the gyro is at rest.

Nevertheless, we can guess that this gyro is very sensitive to time-dependent mechanical stresses. As a matter of fact, after the assembling of the gyro optical parts, we measured the optical output power P = 0.462$\mu$W when $I_f$ = 46mA. This power is higher

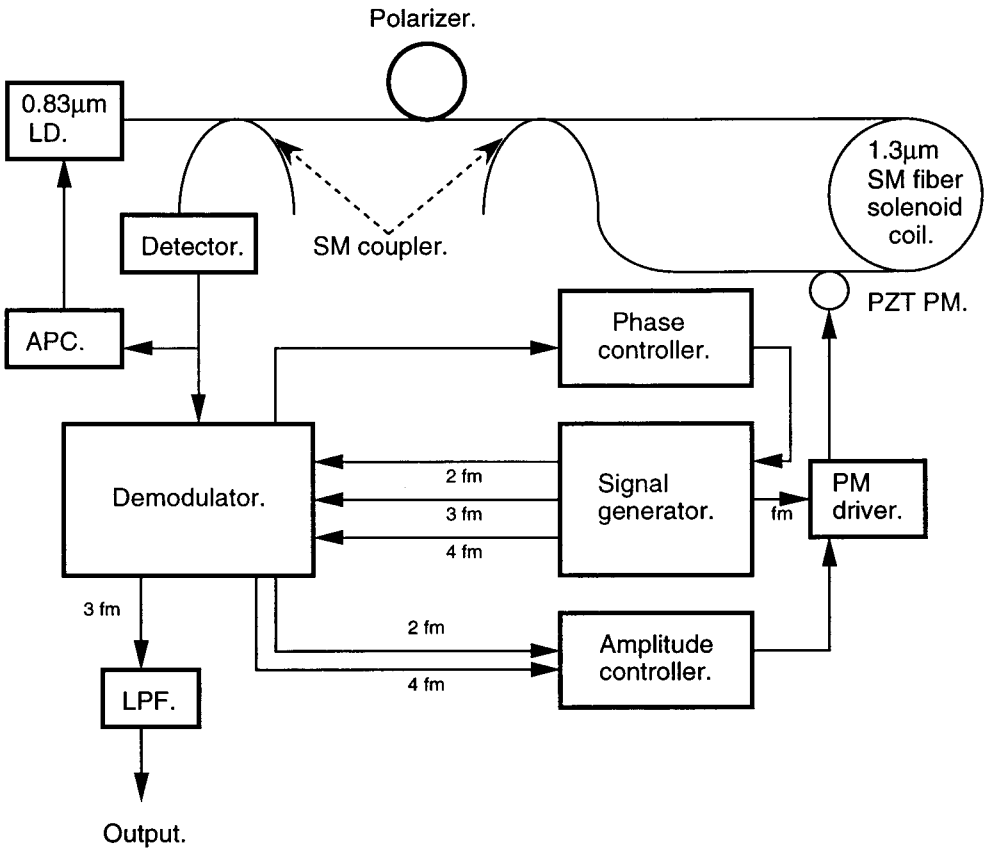


Fig. 28 Third configuration

Table 7 Scale factor test data: case 3

JG-108FA SCALE FACTOR ANALYSIS

| | | | |
|---|---|---|---|
| Assy No. | SANDRA | DATE | '96/07/02 |
| Serial No. | CASE 3 | | |
| OPTICALSENSOR Assy No. | SANDRA | FIBER LENGTH | 180m |
| SENSOR ELEC Assy No. | CASE 3 | | |

| INPUT RATE[°/s] | +25℃ OUTPUT(V) | | −20℃ OUTPUT(V) | | +70℃ OUTPUT(V) | |
|---|---|---|---|---|---|---|
| -100 | -4.766 | | -4.785 | | -4.622 | |
| -90 | -4.300 | | -4.314 | | -4.166 | |
| -80 | -3.825 | | -3.840 | | -3.708 | |
| -70 | -3.350 | | -3.363 | | -3.249 | |
| -60 | -2.875 | | -2.883 | | -2.788 | |
| -50 | -2.396 | | -2.405 | | -2.324 | |
| -40 | -1.916 | | -1.922 | | -1.860 | |
| -30 | -1.437 | | -1.439 | | -1.396 | |
| -20 | -0.955 | | -0.957 | | -0.929 | |
| -10 | -0.474 | | -0.472 | | -0.463 | |
| 10 | 0.490 | | 0.496 | | 0.472 | |
| 20 | 0.972 | | 0.982 | | 0.938 | |
| 30 | 1.453 | | 1.464 | | 1.404 | |
| 40 | 1.935 | | 1.947 | | 1.869 | |
| 50 | 2.414 | | 2.429 | | 2.335 | |
| 60 | 2.892 | | 2.910 | | 2.797 | |
| 70 | 3.370 | | 3.390 | | 3.260 | |
| 80 | 3.846 | | 3.867 | | 3.720 | |
| 90 | 4.319 | | 4.345 | | 4.176 | |
| 100 | 4.789 | | 4.818 | | 4.631 | |
| | | | | | | |
| OFFSET(V) | 0.009 | | 0.012 | | 0.004 | |
| | 0.04793 | | 0.04816 | | 0.04641 | |
| SCALE FACTOR (mV/°/s) | 47.932 | | 48.162 | | 46.414 | |
| TEMPERATURE STAB (±3%) [%] (related to 25℃) | 0.0000 | | 0.4807 | | -3.1669 | |
| LINEARITY ERROR(±1%) [%/FS] | 0.1823 | MAX | 0.1848 | MAX | 0.2223 | MAX |
| | -0.3788 | MIN | -0.3985 | MIN | -0.3310 | MIN |

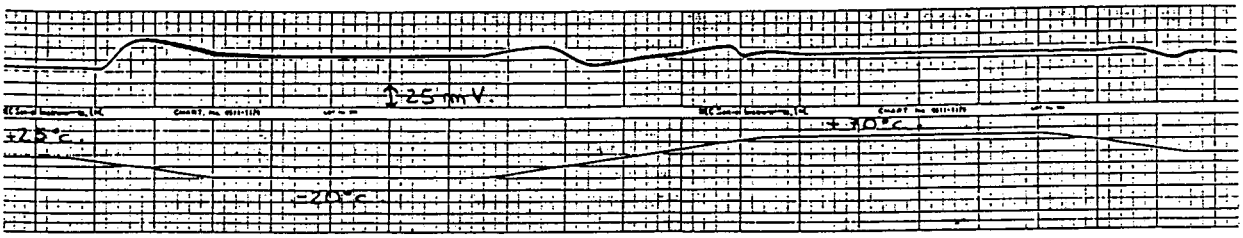


Fig. 29 Bias test data: case 3

than the one in the second case but it varies when the coil fiber is bent.

If the noise requirements are matched according to the bias test data, vibration tests should prove that this configuration has a low environmental ruggedness. After the adjustment of the feedback circuit, the drive current was 33.6mA. It still corresponded to a suitable operating point of the feedback circuit.

(5) Fourth case:

For this fourth case, we removed the polarizer (cf. Fig. 31). The polarizer's leads act as a SM filter and the polarizer provides linearly polarized light to the SM coil. As a consequence, when the polarizer is removed, polarization errors as well as reciprocity errors are generated.

After the assembling of the optical part, we measured the optical output power P = 2.35$\mu$W when $I_f$ = 46mA. This high power level may have required to adapt the circuit gain during the adjustment of the feedback loop but, as it will be proved by the bias test results, this configuration presents too low performance, even when the feedback loop is properly operated, so we did not change the circuit gain. We checked that this optical power level was significantly changed when the fiber from the coil or from the LD was bent. So we can guess that this configuration could not stand mechanical stresses and vibrations.

The bias test confirms that this gyro configuration is too basic to provide suitable performance (cf. Fig. 32). As a matter of fact, the bias drift is about 50°/s as long as the APC circuit manages to control the power level at the detector and then reaches

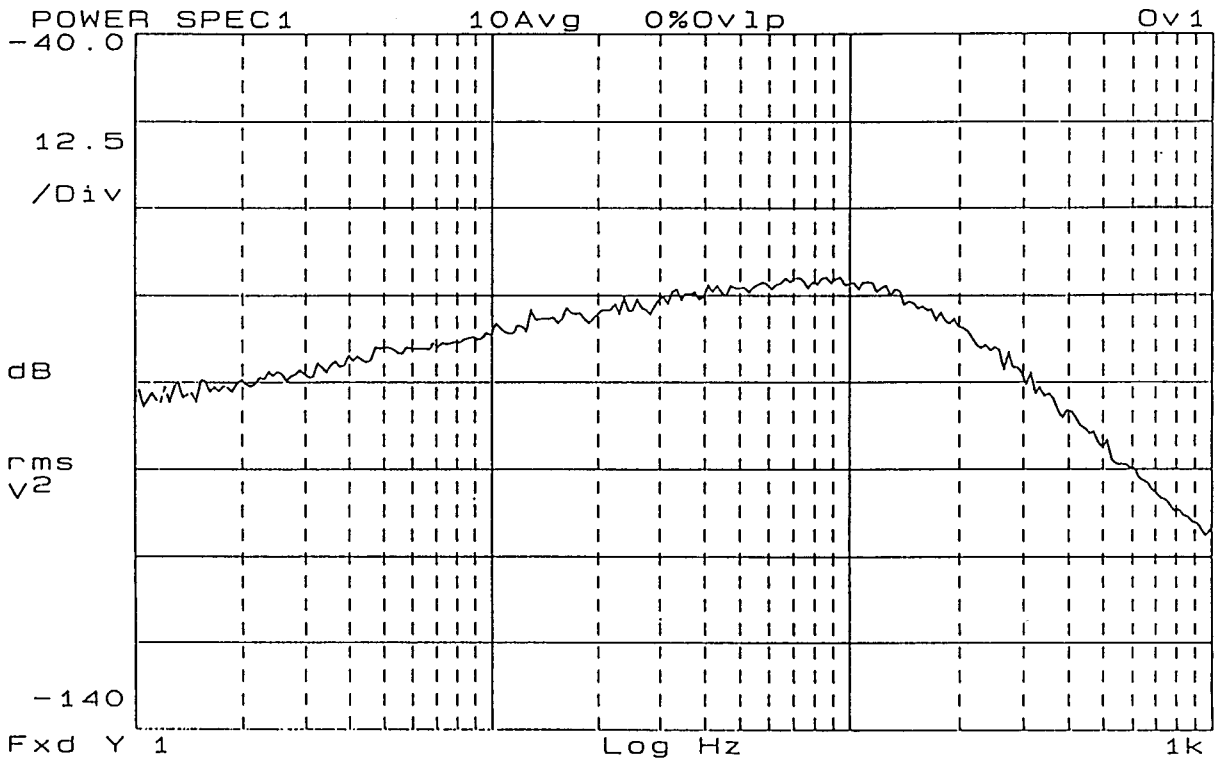


Fig. 30 Spectrum of the gyro's output: case 3

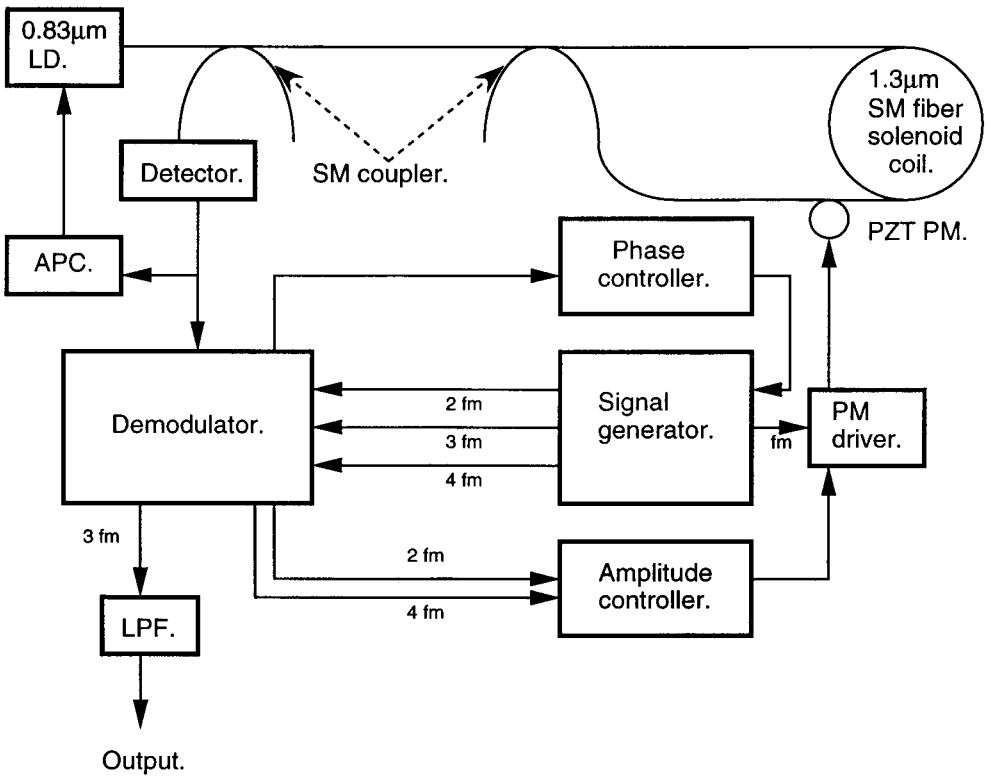


Fig. 31 Fourth configuration.

310°/s when the APC does not manage to compensate the effects of temperature ramping. This configuration cannot be used as a gyro if the temperature is not stable, but this case clearly demonstrated the necessity of a minimum control of the polarization state within the SM coil. For that reason, we could not characterize any scale factor in this case.

### 6.5 Discussion

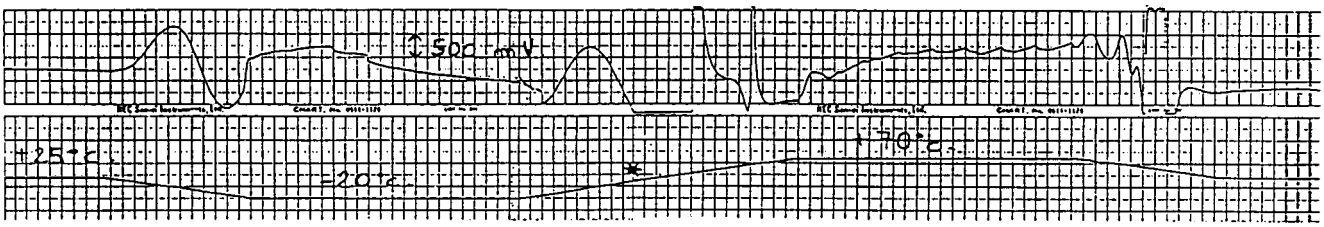


Fig. 32 Bias test data: case 4
(The APC circuit in no longer efficient)

The comparison of these four different configurations of gyro confirms the importance of polarization control on the depolarized gyro performance.

From a theoretical point of view , we can suppose that the phase error generated by polarization errors in the optical part of such a gyro is given by:

$$\phi_e = K\varepsilon P \tag{20}$$

with K: constant
$\varepsilon$: amplitude extinction ratio of the polarizer
$P$: polarization degree of depolarizer 2.

In this case, the rate error is given by :

$$R_e = SF \times \phi_e \tag{21}$$

where $SF = \dfrac{c\lambda}{4\pi Rl}$ is the Sagnac scale factor ($l$ is the length of coil).

Table 8 summarizes the expected results based on this hypothesis and the bias drift data. With K = 0.3, the third and fourth columns are proportional except for the fourth configuration. This validates our hypothesis except for the last case which presents an additional bias drift caused by defects in the modulation and demodulation processes when the APC circuit is no longer efficient. Nevertheless, we should notice that, as long as the APC loop properly compensates the effects of polarization state evolution within the coil, this hypothesis is available : bias drift about 50°/s for the fourth case.

Table 8 Analysis of measured bias data

| | $\phi_e$ (rad) | $R_e$ (°/s) | Bias drift (°/s) |
|---|---|---|---|
| Case 1 | 0.00045×K | 0.1×K | 0.03 |
| Case 2 | 0.00045×K | 0.1×K | 0.02 |
| Case 3 | 0.01×K | 2×K | 0.6 |
| Case 4 | K | 205×K | 310 |

## 7. CONCLUSION

We would compare the perfomances in four different cases and try to establish a production cost / performance balance, and conclude as follows :

1. The fourth case cannot be considered as a gyro.
2. The third one suffers from a drastic degradation of performance compared with the general configuration and the slight reduction of its production cost does not compensate so low performance.
3. The second configuration demonstrated performance equivalent to those of the general configuration and reduces the production cost by the removal of depolarizer 1. In that case, we subtract from the production cost the price of one depolarizer made out of PANDA fiber and also the working time corresponding to two additional splicing points. Vibrations and shocks withstanding tests were not performed on our engineering model but they are necessary before applying this configuration to production. Nevertheless, as bias test data revealed similar behaviors for the two first configurations during temperature ramping, we can trust in the vibrations and shocks withstanding of this second configuration. Moreover, a degradation of vibrations and shocks withstanding would be due to the lack of polarization control in the SM fiber from the LD. So, by tightly fixing this fiber, we could reduce vibrations and shocks sensitivity. Another necessary step before applying to mass production is to establish the distribution of optical components performance so as to make sure that this case is actually representative of the average performance. As future production model of JG-108 FA will use SLD module instead of LD, by operating the SLD at low power level, we might achieve higher light source performance that is to say lower temporal coherence and more evenly split optical power between the two orthogonal axes.

So, finally, this second case seems to be a good candidate for next generation of a low-cost moderate grade I-FOG.

### References

(1) Kazuhiro Sakuma; Application of fiber-optic gyros, OFS-11 Conference Proceedings, 1996.
(2) Hervé Lefèvre; Fundamentals of the interferometric fiber-

optic gyroscope, OFS-11 Conference Proceedings, 1996.

(3) Doug R. Richardson; *Un tour sur la techno des gyros,* Armada International, 3/1995.

(4) Radix J.C.; *Principe de fonctionnement des gyromères à fibres optiques,* poly ENSAE, 1994.

(5) Jeff Duryea, Jeff Bush; Environmental test results of low-cost fiber-optic rate gyros, SPIE vol.2292 Fiber Optic and Laser Sensors XII, 1994.

(6) Laznicka, L. Freier, J. Gilmore, M. Fontanella; I-FOG technology achievements at Draper Laboratory, SPIE vol.2292 Fiber Optic and Laser Sensors XII, 1994.

(7) Mathis, Bruce May, Tom Lasko; Polarization coupling in unpolarized IFOGs: effects of imperfects components, SPIE vol.2292 Fiber Optic and Laser Sensors XII, 1994.

(8) Allen, S.M. Bennett, J. Brunner, R.B. Dyott; A low cost fiber-optic gyro for land navigation, SPIE vol.2292 Fiber Optic and Laser Sensors XII, 1994.

(9) Aritaka Ohno, Ryuji Usui, Kazuo Suzuki, Kenichi Okada, Kazuhiro Sakuma; Intermediate and moderate grade fiber-optic gyroscope for industrial applications, SPIE vol.2292 Fiber Optic and Laser Sensors XII, 1994.

(10) Ryuji Usui, Aritaka Ohno, Kenichi Okada; Intermediate grade FOG with single mode fiber coil, SPIE vol.2070 Fiber Optic and Laser Sensors XI, 1993.

(11) Deepak Uttamchandani, Ivan Andonovic; *Principles of modern optical systems,* volume II, Artech House, 1992.

(12) Aritaka Ohno, Shinji Motohara, Ryuji Usui, Yuji Itoh, Kenichi Okada; Development of fiber-optic gyroscope with environmental ruggedness, SPIE vol.1585 Fiber Optic Gyros : 15th Anniversary Conference, 1991.

(13) Bogdane Szafraniec, John Feth, Ralph Bergh, James Blake; Performance improvements in depolarized fiber gyros, SPIE vol.2510.

(14) Hervé Lefère; *Principe du gyrofibre, le gyromère des futures applications à haute dynamique,* Revue Scientifique et Technique de la Défense, 1er trimestre 1990.

(15) Robert B. Smith; *Selected papers on fiber-optic gyroscopes,* SPIE Milestone Series, vol. MS8, 1989.

(16) Konrad Bohm, Klauss Petermann, Edgar Weidel; Performance of Lyot depolarizers with birefringent single-mode fibers, Journal of Lightwave Technology, vol. LT-1, no.1, march 1983.

**航空宇宙技術研究所資料 709T 号**

平成 9 年 3 月発行

発行所 航空宇宙技術研究所
東京都調布市深大寺東町 7 丁目 44 番地 1
電話三鷹(0422)47-5911(大代表)〒 182

印刷所 株式会社 東京プレス
東京都板橋区桜川 2 − 27 − 12

Printed in Japan